Terrane boundary reactivation, barriers to lateral fault propagation and reactivated fabrics - Rifting across the Median Batholith Zone, Great South Basin, New Zealand

Thomas B. Phillips*; Ken J. McCaffrey

Department of Earth Sciences, University of Durham, Science labs, Elvet Hill, Durham, DH1 3LE

thomas.b.phillips@durham.ac.uk

Key points

- We document multiple styles of structural inheritance influencing aspects of rift physiography in the Great South Basin, New Zealand
- The southern boundary of the Median Batholith Zone terrane is reactivated as a large extensional shear zone and detachment
- Faults splay, segment and eventually terminate as they approach stronger material associated with a granitic laccolith.

Abstract

Prominent structural heterogeneities within the lithosphere may localise or partition strain and deformation during tectonic events. The NE-trending Great South Basin, offshore New Zealand, formed perpendicular to a series of underlying crustal terranes, including the dominantly granitic Median Batholith Zone, which along with boundaries between individual terranes, exert a strong control on rift physiography and kinematics. We find that the crustal-to-lithospheric scale southern terrane boundary of the Median Batholith Zone is associated with a crustal-scale shear zone that was reactivated during Late Cretaceous extension between Zealandia and Australia. This reactivated terrane boundary is oriented at a high-angle to the faults defining the Great South Basin. We identify a large granitic laccolith along the southern margin of the Median Batholith, expressed as sub-horizontal packages of reflectivity and acoustically transparent areas on seismic reflection data. The presence of this strong granitic body inhibits the lateral propagation of NE-trending faults, which segment into a series of splays that align along the margin as they approach. Further, we also identify two prominent E-W and NE-SW oriented fabrics within the basin, which are exploited by small-scale faults across the basin.

We show how different mechanisms of structural inheritance are able to operate simultaneously, and somewhat independently, within rift systems at different scales of observation. The presence of structural heterogeneities across all scales need to be incorporated into our understanding of the structural evolution of complex rift systems.

1. Introduction

Continental crust typically grows through the amalgamation of crustal terranes and the intrusion of igneous plutonic material. As a result, pre-existing structural heterogeneities are present throughout the lithosphere and exert a considerable influence over the development of rift systems across all scales. Individual crustal terranes contain numerous internal structural heterogeneities that reflect their unique tectonic histories, whilst the boundaries with adjacent terranes form pronounced crustal-to-lithosphere scale rheological and lithological contrasts (Howell 1980; McWilliams & Howell 1982; Bishop et al. 1985; Mortimer 2004; Lundmark et al. 2013; Peace et al. 2017; Johnston 2019).

Lithospheric-scale structures often localise strain, for example in orogenic belts surrounding cratonic continental interiors, and can control the location of rift systems and, to some extent, continental breakup (Wilson 1966; Dore et al. 1997; Tommasi & Vauchez 2001; Thomas 2006; Paton et al. 2016; Wenker & Beaumont 2016; Phillips et al. 2018; Thomas 2018; Heron et al. 2019). In rift systems, pre-existing structures in the crust may localise deformation and control the geometry and evolution of individual faults (Daly et al. 1989; Fossen et al. 2016; Mortimer et al. 2016; Phillips et al. 2016; Fazlikhani et al. 2017; Morley 2017; Peace et al. 2017; Dawson et al. 2018; Rotevatn et al. 2018b; Vasconcelos et al. 2019). Areas of stronger material, such as intruded plutons or stronger terranes may also inhibit fault nucleation and propagation, influencing the geometry of individual faults and the physiography of the overall rift (Critchley 1984; Koopmann et al. 2014; Magee et al. 2014; Peace et al. 2017; Howell et al. 2019). At the outcrop scale, pre-existing structures and fabrics may be exploited by later faults and fractures (Morley et al. 2004; Paton & Underhill 2004; De Paola et al. 2005; Morley 2010; Chattopadhyay & Chakra 2013; Kirkpatrick et al. 2013; Duffy et al. 2015; Dichiarante et al. 2016; Mortimer et al. 2016; Phillips et al. 2017). This multitude of pre-existing structures exert a range of influences over extensional processes, however, an understanding of how these different structural heterogeneities are expressed in rift systems, how they link across scales and how they affect various aspects of rift physiography is currently lacking.

In this study, we focus on the Great South Basin, a NE-trending rift system located offshore the South Island of New Zealand. Basement beneath the basin comprises a series of volcano-sedimentary terranes, which accreted along the southern margin of Gondwana during protracted Cambrian-Cretaceous subduction (Mortimer et al. 1999; Tulloch et al. 1999; Mortimer 2004, 2014; Robertson et al. 2019; Robertson & Palamakumbura 2019; Tulloch et al. 2019). These terranes are separated by W- to WNW-trending crustal-to-lithospheric scale boundaries that are oriented perpendicular to the overlying basin (Muir et al. 2000; Mortimer et al. 2002). We focus on the evolution of the basin atop the Median Batholith Zone, a Carboniferous-Early Cretaceous Cordilleran-style magmatic arc, and its boundaries with the Western Province terranes to the south and the Brook Street and Murihiku Terranes to the north (Figure 1) (Bishop et al. 1985; Tulloch et al. 1999; Mortimer et al. 2002; Jongens 2006; Tulloch et al. 2019).

Based on borehole-constrained 2D and 3D seismic reflection data, we document multiple structural heterogeneities beneath the Great South Basin, and determine how they influence rift physiography and kinematics throughout multiple tectonic events. The framework provided by these pre-existing structures variably influences rift physiography across different scales of observation, from controlling rift segmentation and the location of sub-basins, to controlling the geometry and kinematics of individual fault systems.

2. Regional geological setting and evolution

The Great South Basin is a NE-trending rift basin located offshore of the east coast of the South Island of New Zealand. It contains a maximum sedimentary thickness of 8.6 km, which includes up to 4 km of Upper Cretaceous strata (Beggs 1993; Sahoo et al. 2014; Morley et al. 2017) (Figure 1, 3). The Great South Basin, along with the adjacent Canterbury Basin and Bounty Trough, is situated within the Campbell Plateau, a submerged (<1000 m water depth) area of thinned continental crust (~22 km) that extends ~1000 km southeast of the South Island (Figure 1) (Beggs 1993; Mortimer et al. 2002; Grobys et al. 2009; Uruski 2010; Higgs et al. 2019). Here, we focus on a 21,000 km^2 area covering the southern part of the Great South Basin, located to the southeast of Stewart Island (Figure 1).

The basement geology of New Zealand comprises a series of crustal to lithospheric terranes that accreted to the southern margin of Gondwana during protracted subduction from the Cambrian-Early Cretaceous (Bishop et al. 1985; Bradshaw 1989; Muir et al. 2000; Mortimer 2014). Subduction ceased during the Early Cretaceous (~105 Ma) as the buoyant Hikurangi Plateau collided along the margin (Davy et al. 2008; Uruski 2015). Since the Cenozoic, these terranes have been offset along the Alpine Fault, a major plate boundary and strike-slip fault located along the spine of the South Island that has accommodated ~480 km offset (Wellman 1953; Cooper et al. 1987; Sutherland et al. 2000). Due to this offset, the basement terranes of the South Island are also present beneath the North Island (Figure 1) (Muir et al. 2000; Mortimer et al. 2002; Collanega et al. 2018). The basement terranes are divided into Eastern and Western provinces separated by the Median Batholith Zone. The timing of accretion along the Gondwana margin becomes younger eastwards, with those terranes of the Western Province terranes accreting to the margin of Gondwana earlier than those in the Eastern Province and occupying a more proximal position with respect to the continental interior. Here, we focus on those terranes that underlie the Great South Basin, the Western Province Terranes, the Median Batholith Zone and the Brook Street and Murihiku terranes of the Eastern Province (Figure 1).

The Western Province comprises the Buller and Takaka terranes, which represent a Gondwana-derived continental fragment accreted along the margin during the Cambrian-Devonian (Bradshaw 1989; Mortimer 2004; Bache et al. 2014; Tulloch et al. 2019). The Eastern Province terranes largely originated within the Panthalassa Ocean as a series of volcanic and magmatic arcs and associated sedimentary basins (Bishop et al. 1985; Mortimer et al. 1997; Mortimer et al. 2002; Mortimer 2004). The Brook Street terrane is immediately north of the Median Batholith and comprises a Permian volcanic and volcaniclastic sequence that initially formed as an intra-oceanic arc (Landis et al. 1999; Mortimer 2004). Further north, the Murihiku terrane is composed of gently folded Jurassic-aged sandstones and volcaniclastic rocks that were initially part of a forearc sedimentary basin (Campbell et al. 2003; Mortimer 2004). Between the Western and Eastern Province terranes is the Median

Batholith Zone, a Cordilleran-style magmatic arc that represented the site of subduction-related magmatism from 375-110 Ma (Mortimer et al. 1999; Mortimer 2004). Although previously interpreted as a highly tectonised allocthonous zone, recent studies have demonstrated that the majority of plutonic material is autochthonous, with only relatively minor reworking and tectonism identified. Hence, we refer to the structure as the Median Batholith Zone (Mortimer et al. 1999). The Median Batholith Zone comprises numerous plutonic intrusions that can be divided into various suites based on the age of emplacement and composition (Tulloch 1988; Allibone & Tulloch 2004). An overall southwards younging trend occurs across the batholith (Mortimer et al. 1999; Allibone & Tulloch 2004), with the Cretaceous-aged Separation Point Batholith suite located along the southern margin of the zone and older batholith suites towards the northern margin (Muir et al. 2000; Allibone & Tulloch 2004).

The Great South Basin formed via two phases of extension during the Late Cretaceous related to the breakup of Gondwana. Extensional activity may have begun in the Jurassic-Early Cretaceous in a back-arc setting along the southern margin of Gondwana, with Jurassic strata identified in the deepwater Taranaki Basin and potentially in the Great South Basin (Grobys et al. 2007; Uruski et al. 2007; Uruski 2010). Initial NE-SW oriented extension occurred between Australia and the contiguous Zealandia and Western Antarctica at ~101-89 Ma related to the opening of the Tasman Sea and the northwards propagation of the Tasman ridge (Kula et al. 2007; Kula et al. 2009; Sahoo et al. 2014; Tulloch et al. 2019). A second rift phase, related to the breakup of Zealandia and Western Antarctica and associated with the formation of the Pacific ridge, occurred at 90-80 Ma (Kula et al. 2007; Tulloch et al. 2019). Extensional stresses were oriented NW-SE, roughly parallel to the underlying basement terrane boundaries, and resulted in the formation of the NE-trending Great South Basin (Figure 1). Late Cretaceous extension, forming the Great South and Canterbury basins and the Bounty Trough greatly reduced the crustal thickness in the area to around 22 km (Mortimer et al. 2002). In the Great South Basin, faults related to this activity have been proposed to sole out onto a mid-crustal detachment (Uruski et al. 2007; Sahoo et al. 2014).

The onset of subduction in the Tonga-Kermadec region in the Oligo-Miocene and the formation of the Alpine Fault resulted in a regional compressional regime across New Zealand (Cooper et al. 1987; Sutherland et al. 2000; Sutherland et al. 2010; Bache et al. 2012). The Great South Basin was relatively far-removed from the compressional stresses associated with the formation of this new plate boundary, with regional compression expressed as low-amplitude, long wavelength folding (Uruski 2010).

3. Data and Methods

3.1 Seismic interpretation

We use borehole-constrained 2D and 3D seismic reflection data, covering an area of 21,000 km^2 offshore of the South Island of New Zealand. A 3D seismic reflection volume (GSB-3D) was acquired in the south of this area and covers ~1,400 km^2 (Figure 1). Seismic reflection data follow the SEG normal polarity convention; that is, a downwards increase in acoustic impedance (i.e. the seabed) is represented by a peak, whereas a downwards decrease in acoustic impedance is represented by a trough (Figure 2). 2D seismic reflection data record to 6-8 s TWT and display variable image quality between individual surveys. The 3D seismic volume records to 8 s TWT and displays excellent image quality throughout.

The ages of regional stratigraphic horizons were constrained by the nearby Pukaki-1, Pakaha-1, Tara-1, Toroa-1 and Rakiura-1 boreholes (Figure 1). We mapped a series of prominent seismic reflections throughout the dataset and linked them to the regional stratigraphy (Figure 2). A seismic-well tie was performed on the Pukaki-1 well to link the seismic interpretations to the well data (Figure 2). A well-tie was not performed on the Pakaha-1 well due to a lack of coverage by wireline log data. Top Acoustic Basement and intra-Upper Cretaceous horizons form the main surfaces referred to throughout this study (Figure 2). Top Acoustic Basement typically represents top crystalline basement across the area (Figure 1), although in some instances, bedding-related reflectivity is observed beneath this surface, potentially indicative of earlier activity (Figure 3). North of the study area, basement of the Murihiku terrane consists of allocthonous Permian to Early Cretaceous-aged sedimentary strata, where present these strata are classified as acoustic basement (Bache et al. 2014; Tulloch et al. 2019). The intra-Upper Cretaceous horizons was interpreted throughout the 3D seismic volume and across the main basin depocentre to map syn-rift fault geometries in more detail (Figure 1, 3). Shallower horizons are also interpreted in the post-rift interval, although these provide little information on the structural evolution of the basin (Figure 2, 3). Seismic interpretations were carried out, and are presented, in the time domain (seconds Two-way-travel time; s TWT). Key structural measurements were converted to the depth domain based on regional checkshot information.

Crystalline basement in the area is mostly associated with the underlying Median Batholith (Figure 1). The Pakaha-1 well penetrates a granitic basement dated at ~323 Ma that is interpreted to represent Carboniferous basement to the Median Batholith (Figure 4) (Tulloch et al. 2019). The Pukaki-1 well penetrates further granitic basement to the southeast (Figure 1). This granite is dated at 107 Ma and can be confidently correlated with the Separation Point Batholith suite (Tulloch et al. 2009; Tulloch et al. 2019). The Separation Point Batholith suite is also identified in the same structural setting, along the boundary between the Median Batholith and Western Province terranes, in the North Island (Muir et al. 2000).

3.2 Quantitative fault analysis

We performed quantitative analyses, in the form of throw-length plots, on a series of faults within the basin to quantify their geometric and kinematic evolution. The geometry of each fault analysed, including horizon cutoffs and any tip lines were carefully constrained throughout the data to minimise any interpretation-related artefacts (Walsh et al. 2003; Duffy et al. 2015). Based on our fault interpretations we calculated throw-length plots for individual fault segments at both the Acoustic Basement and intra-Upper Cretaceous stratigraphic horizons. To accurately constrain the kinematic evolution of a fault we need to record all fault slip-related strain, including both brittle faulting and ductile folding such as that associated with fault propagation folding. Therefore, horizon cut-offs were projected to the fault plane from an area unaffected by local fault parallel folding (Walsh et al. 1996; Long & Imber 2012; Whipp et al. 2014; Duffy et al. 2015; Coleman et al. 2018)

Throw measurements were taken along a series of parallel seismic sections oriented orthogonal to the main fault trend, each separated by ~339 m. Analyses of individual faults were then collapsed onto a single plane representing a strike projection of the overall fault system. This allowed us to calculate the cumulative throw accrued across the fault system and to analyse how strain was accommodated along its length.

4. Rift physiography

In this section, we describe the overall rift physiography of the study area. We first describe the regional geometry of the Great South Basin across the Acoustic Basement surface, before describing the detailed fault and rift geometry, at both the Acoustic Basement and intra-upper Cretaceous structural levels, using the 3D seismic volume in the centre of the basin (Figure 1).

4.1 Regional rift geometry

The Great South Basin is characterised by NE-trending, predominantly SE-dipping faults. NW-dipping faults are also present and help define a series of NE-trending basement ridges in the east of the area (Figure 1). The centre of the basin reaches 3-4 s TWT (~4.5 km) depth and shallows eastwards onto the continental shelf (~1.5 s TWT, ~1.3 km) (Figure 1, 3). The basin deepens to around 5 s TWT (~9 km) in the north and the south (Figure 1).

Upper Cretaceous syn-rift strata thicken into the hangingwalls of major NE-trending faults (Figure 3), indicating Late Cretaceous activity along these structures. We also recognise a potentially earlier phase of activity, with apparent syn-rift strata present below the acoustic basement surface in the hangingwalls of some structures (Figure 3). Although we are unable to assign an age to these strata, we suggest that, based on regional considerations, they are likely Late Jurassic-Cretaceous in age

(Uruski et al. 2007; Uruski 2010). Palaeocene to recent strata comprise the post-rift basin fill and display a slight westwards thickening related to increased sediment input and clinoform progradation from the mainland (Figure 3). A large clinoform sequence at the seafloor forms a major bathymetric escarpment to the west (Figure 3). E-dipping faults along the western margin of the basin appear to merge at depth, potentially reflecting the listric geometry observed elsewhere (Uruski et al. 2007) (Figure 3). In the east of the area, the Pakaha-1 well penetrates granitic basement atop a ~10 km wide NE-trending horst termed the Pakaha Ridge (Figure 1). Basement beneath this ridge is highly reflective and appears to dip westwards. A series of W-dipping faults define the western margin of this ridge and appear to merge with the basement reflectivity at ~5-6 s TWT (~10.5 km) (Figure 3).

A major WNW-trending, SSW-dipping fault is identified in the south of the area, and is associated with a large WNW-ESE oriented depocentre (~5 s TWT; 9 km depth) in its hangingwall (Figure 1). This structure is co-located with the boundary between the Median Batholith Zone and the Western Province Terranes, and is henceforth termed the Terrane Boundary Fault (Figure 1). A WNW-trending structural high is present in the footwall of the Terrane Boundary Fault, defining a relatively unfaulted area bound to the south by the Terrane Boundary Fault and to the north by WNW-trending, NE-dipping faults (Figure 1, 4a). The structural high appears to link into the Pakaha ridge to the east. We henceforth refer to this structural high as the Terrane Boundary Fault (TBF) Footwall Block (Figure 1, 4).

4.2 Detailed basin geometry – 3D seismic volume

Two horizons mapped through the 3D seismic volume provide additional detail on the fault geometries and rift physiography in the centre of the basin (Figure 4). Two NE-striking, SE-dipping faults are present at the Acoustic Basement surface in the north of the area (Figure 4a). The northernmost fault forms the northern boundary to the main basin depocentre (Figure 1, 3, 4a). The other fault forms a single structure in the northeast that splays into series of smaller segments to the southwest and is referred to as the 'Splaying Fault System'. Individual segments of the Splaying Fault System dip southeast and northwest, resulting in complex plan-view geometries and non-resolvable cross-cutting relationships at depth (Figure 3, 4a). As they approach the northern margin of the TBF Footwall Block in the southwest, the segments rotate around vertical axes to a more WNW orientation and terminate along the boundary of the TBF Footwall Block (Figure 4). The TBF Footwall Block itself is relatively unfaulted; with only a few minor WNW- and NE-trending faults present (Figure 4a). Although the northern margin of the TBF Footwall Block is largely parallel to the Terrane Boundary Fault, a series of embayments are present along its southern margin, in the immediate footwall of the fault (Figure 4a). These embayments are typically 5-8 km wide and incise about ~6 km back into the TBF Footwall Block.

The complex geometry of the Splaying Fault System is further highlighted across the intra-Upper Cretaceous surface (Figure 4b). The footwall of the main fault is cross-cut by a series of SE and NW-dipping faults to the southwest, with some NW-dipping antithetic faults also developing in the hangingwall. Individual segments of the Splaying Fault system rotate to a more WNW-trending orientation as they approach the TBF Footwall Block (Figure 4b). Horsetail splay geometries are identified along-strike of the main fault, where both NW- and SE-dipping fault segments diverge and rotate to become NE-dipping (Figure 4b).

Some NE-striking, SE-dipping faults are present to the southwest of the area, defining a series of NE-trending structural highs superimposed atop the TBF Footwall Block (Figure 4b). The Terrane Boundary Fault is not clearly expressed at this structural level, although a few minor WNW-trending, SSW-dipping faults are present along the southern margin of the WNW-block (Figure 4b).

5. Styles of structural inheritance

5.1 Terrane boundary reactivation

The Terrane Boundary Fault forms a ~65 km long structure across the southern margin of the area and is coincident with the boundary between the Median Batholith Zone and the Western Province terranes (Figure 1). The fault dips SSW, away from the Median Batholith Zone, and records >1 s (>2 km) of throw across the Acoustic Basement surface (Figure 5, 6).

The Terrane Boundary Fault corresponds to a prominent reflection on seismic data, with a package of high-amplitude inclined reflections present in its footwall. This package of reflections is truncated by the top Basement surface and extends to lower crustal depths (8 s TWT; ~20 km) (Figure 5, 6). Internal reflections are remarkably continuous within the package, spanning depth intervals of >2.5 s (Figure 5). The width of the reflection package increases at shallower depths, from ~2 km wide at 6-7 s TWT (~15 km), to ~5 km wide at 2-3 s TWT (~2.7 km) (Figure 5, 6). A reflection corresponding to the lower boundary of this package can be traced to the top Acoustic Basement surface, where the package delineates a 5-7 km wide subcrop at the top Acoustic Basement surface (Figure 5).

A series of faults merge with the Terrane Boundary Fault downdip, defining a series of fault blocks that show increasing offset along the fault with depth (Figure 5). The timing of activity along these faults appears to migrate updip along the structure, with deeper faults showing earlier activity than those at shallow depths (Figure 5). In some areas, the fault plane becoming sub-horizontal at shallower depths, creating a series of embayments that extend northwards into the footwall of the Terrane Boundary Fault and the TBF Footwall Block (Figure 4, 7). Fault blocks within these embayments detach onto the top reflection of the reflection package and show south-directed transport downdip (Figure 6, 7).

In addition to the inclined reflection package associated with the footwall of the Terrane Boundary Fault, we also observe packages of high-amplitude reflectivity at mid-crustal depths (4-6 s TWT; 6-12 km) which extend beneath the TBF Footwall Block. These reflection packages are typically sub-horizontal although they may dip slightly northwards further to the north (Figure 5, 6). Beneath the platform to the west, these reflection packages define areas of high- and low-reflectivity within crystalline basement that extend from 3-6 s TWT (3.5-12.5 km) (Figure 5). Beneath the basin, the packages display a more domal geometry and are present from 5-7 s TWT (9-16.5 km) (Figure 6). In both instances, the packages merge with those associated with the Terrane Boundary Fault and are only present in its footwall.

Based on its geometry and seismic reflection character, we interpret the high-amplitude and coherent package of intra-basement reflectivity in the footwall of the Terrane Boundary Fault as representing a shear zone (termed the Terrane Boundary Shear Zone). The seismic character of the intrabasement reflectivity resembles that of shear zones identified elsewhere in seismic data. In these other examples, the shear zone interpretation can be independently verified through links to structures identified onshore (Freeman et al. 1988; Wang et al. 1989; Phillips et al. 2016; Fazlikhani et al. 2017; Lenhart et al. 2019) or encountered in boreholes (Hedin et al. 2016). The characteristic intra-basement reflectivity forms through constructive interference between highly deformed mylonite zones and intervening relatively undeformed material (Jones & Nur 1984; Carreras 2001; Reeve et al. 2013; Rennie et al. 2013; Phillips et al. 2016). We interpret the prominent reflection at the top of the shear zone as a detachment horizon, potentially exploiting a relatively weak mylonitic zone.

We interpret the sub-horizontal reflection packages in the footwall of the Terrane Boundary Shear Zone to represent a series of granitic laccolith intrusions. Granitic material is present in this area due to our location within the Median Batholith Zone (Mortimer et al. 1999; Tulloch et al. 2019). Our interpretation is further corroborated by granitic basement in the nearby Pakaha-1 and Pukaki-1 boreholes (Figure 1). In addition, the reflection character within basement of the likely granitic Pakaha Ridge resembles that identified here (Figure 3, 6), with the Pakaha Ridge also potentially joining with the TBF Footwall Block in the east of the area (Figure 1). Granitic plutons belonging to the Separation Point Batholith suite are identified between the Western Province Terranes and the Median Batholith Zone beneath the Taranaki Basin, offshore of the North Island (Mortimer et al. 1997; Muir et al. 2000). Furthermore, the reflection patterns observed here, of sub-horizontal packages of high- and low- amplitude packages of reflectivity, resemble those observed from the Lake District Batholith, where prominent reflections are generated at the boundaries of stacked granite laccoliths (Figure 5) (Evans et al. 1993; Evans et al. 1994). The interpreted reflection packages also display a lenticular geometry, consistent with those expected from granitic intrusions (McCaffrey & Petford 1997; Petford et al. 2000). At the top Acoustic Basement structural level, this granite underpins the relatively unfaulted TBF Footwall Block (Figure 4). In the platform area, a prominent package of reflections at ~6 s TWT (~12 km) depth may be interpreted as the base of the granite batholith, with the lenticular granite bodies extending upwards to ~3 s TWT (~3.5 km) (Figure 5).

Further east, the top of the granitic body appears to be situated at shallower depths (~5 s TWT; ~9 km) (Figure 6).

5.2 Strong crustal blocks as barriers to fault propagation

As outlined in the previous section, we propose that a granitic body (Figure 3) underlies the relatively unfaulted TBF Footwall Block. To the north, the NE-trending Splaying Fault System abuts against and terminates at the Footwall Block to the southwest (Figure 4). Reflectivity associated with the NE-trending Splaying Fault systems cross-cuts the granite-related reflectivity in the footwall of the Terrane Boundary Fault, indicating that activity along the Splaying Fault system occurred after the Footwall block was established (Figure 6, 7). We now describe in detail how the geometry of the Splaying Fault System changes from NE to SW, towards the TBF Footwall Block.

In the northeast of the area, away from the TBF Footwall Block, strain is accommodated by a single fault (Figure 8a). Evidence of earlier activity is also present in this area, with the identification of bedding- and fault-related reflectivity beneath the Acoustic Basement surface (Figure 8a). Any pre-Acoustic Basement strata is likely to be Jurassic to Early Cretaceous in age, relating to the earliest stages in the basin's formation (Uruski et al. 2007; Uruski 2010). Approaching the WNW-trending TBF Footwall Block to the southwest, the fault begins to splay into a series of SE- and NW-dipping faults synthetic and antithetic to the main fault respectively (Figure 4b, 8b). This fault segmentation is initially accommodated by dissection of the footwall into four fault segments that merge to a single structure at depth, and by the formation of a series of antithetic faults in the hangingwall (Figure 8b). The antithetic faults also appear to abut against the main fault structure at depth, although detailed cross-cutting relationships cannot be identified in the data. Additional NW-dipping faults form in the footwall of the main fault, dipping away from the structure and further bisecting the footwall (Figure 8b). As the fault continues to the southwest, the footwall becomes very highly deformed by both SE- and NW-dipping faults such that no dominant fault or overall hangingwall and footwall can be identified (Figure 8c). At this distance along the fault, extension is accommodated by multiple faults across a ~15 km wide zone (Figure 8c). Pre-acoustic basement sedimentary strata are again identified in this area, although no divergent stratal wedges are identified in the hangingwalls of the segments of the Splaying Fault, indicating that it was not active at that time (Figure 8c). However, we do identify pre-acoustic basement syn-rift strata in the hangingwalls of the major faults to the northwest and southeast of the Splaying Fault system (Figure 8a, 8b). As the Splaying Fault System approaches the TBF Footwall Block, extension is accommodated by a complex system of NW- and SE dipping faults (Figure 8d). The dominant fault appears to switch in this location, with a NW-dipping fault seemingly cross-cutting the SE-dipping fault that is dominant along-strike to the northeast (Figure 8d). The main segments of the splaying fault begin to rotate to a WNW-striking orientation, dipping to the northeast (Figure 4b). The rotation of these faults appears to be at least partially accommodated by the upwards splaying of the faults (Figure 8d). A series of NW-dipping faults to the east of the Splaying Fault merge into a package of reflectivity at depth and join with an additional fault to the east that forms the border to a basement ridge (Figure 4, 8d). The geometry and structural style of these faults resemble those along the western border of the Pakaha ridge, where multiple faults root onto the margin of a granitic basement ridge (Figure 3, 8d).

By measuring throw across individual segments within the Splaying Fault System we are able to quantitatively analyse how strain is accommodated along the length of the fault; from the single structure in the northeast, to the wider zone of deformation proximal to the TBF Footwall Block in the southwest. In the northeast, throw across both the Acoustic Basement and Intra-upper Cretaceous surfaces is accommodated by a single fault, accounting for ~800 ms (~1.8 km) and ~250 ms (~200 m) throw across each surface respectively (Figure 9, 10). Two throw minima are present along the throw profile, corresponding to bends in the fault trace and representing relay ramps along the fault (Figure 4, 9). Throw across the top Acoustic Basement surface decreases to the southwest at around 15 km along the fault, as extension is accommodated by a series of smaller segments in the footwall and hangingwall, each accommodating 100-200 ms throw (~200 m) (Figure 9). One notable feature is that as the fault splays and the dominant fault in the northeast terminates, the cumulative throw across the whole system remains relatively constant. To the southwest, extension is accommodated by more numerous, lower displacement segments (Figure 9). The relatively constant cumulative throw along the system indicates that the strain and applied stress is constant along the length of the fault and that the degree of maturity of the fault is not responsible for its segmentation and splaying geometry (cf. Nixon et al. 2014).

A cumulative throw minimum is present at ~24 km along the length of the fault at the Acoustic Basement structural level. However, this appears to be related to a lack of imaging of faults in this area rather than a property of the system itself (Figure 9). To the southwest, the individual fault segments rotate to a more WNW-orientation and terminate at the northern margin of the TBF Footwall Block (Figure 4a). At the boundary of the TBF Footwall Block, cumulative throw decreases from ~600 ms to zero over a distance of ~1 km, leading to a large gradient in the cumulative fault throw.

Throw analyses across the Intra-upper Cretaceous surface tell a similar story to the Acoustic Basement surface (Figure 10). Individual fault segments are better resolved across this surface meaning that they may provide a more complete record of the distribution of strain along the Splaying Fault system (Figure 10). As across the Acoustic Basement surface, throw is initially accommodated by a single, segmented fault in the northeast (Fault 1; Figure 10), which records 250-350 ms (~250 m) throw. To the southwest, throw across this fault drastically decreases with throw being accommodated by at least 20 smaller segments. At around 11 km along the Splaying Fault system, a new fault (F2; Figure 10) forms in the hangingwall of Fault 1 and initially accommodates around ~150 ms (~200 m) throw compared to 25-50 ms (~50 m) throw across Fault 1 in the same location. In the northeast, Fault 1 appears to have been associated with a period of fault propagation folding prior to the brittle offset of the intra-upper Cretaceous surface, which is incorporated into our throw analyses (Figure 8a). When F2 forms in the hangingwall of Fault 1, it records the ductile deformation rather than Fault 1, now located in the footwall of F2 (Figure 10). Further southwest, extension is accommodated by multiple, low-displacement splays (~50 ms throw), which produce a relatively constant cumulative throw across the whole Splaying Fault System (~200 ms) (Figure 10). In contrast to the Acoustic Basement surface, we do not identify a prominent minimum along the fault splays (~24 km) (Figure 10). As the Splaying Fault system approaches the northern margin of the TBF Footwall Block, individual segments begin to rotate to align with the margin and terminate (Figure 4b, 10). At the northern margin of the TBF Footwall Block, cumulative throw across the system decreases from ~150 ms to ~50 ms over a distance of 1-2 km, forming a relatively high displacement gradient (Figure 10). Some low-displacement faults (~20 ms throw) propagate into the TBF Footwall Block (Figure 10).

In the northeast, the Splaying Fault System is characterised by a singular fault plane, resembling a relatively typical fault associated with Late Cretaceous rifting in the Great South Basin (Uruski et al. 2007; Sahoo et al. 2014). No major faults are present across the TBF Footwall Block to the southwest. As the Splaying Fault approaches this block it begins to splay into a series of relatively low-displacement segments. Those segments emanating from the footwall of the main fault display a divergent geometry, dipping away from the main fault, whereas those in the hangingwall appear to form a more convergent geometry (Figure 4, 10). We propose that the granite-cored TBF Footwall Block represents an area of stronger material that inhibits fault nucleation and acts as a barrier to lateral fault propagation.

We observe complex fault geometries along the northern margin of the TBF Footwall Block (Figure 11). Horsetail splay type geometries are situated at the terminations of Faults 15 and 16 across the intra-upper Cretaceous surface (Figure 11). NE trending faults rotate sharply to NW and S/SE orientations at the boundary of the TBF Footwall Block, whilst also splaying into a series of segments that define small-scale graben structures (Figure 11). The graben structures are oriented parallel to the northern margin of the TBF Footwall Block and seemingly parallel to the prevailing extension direction (Figure 11). Faults defining these graben appear to originate from a single point located at a deeper structural level and are only expressed across the intra-upper Cretaceous surface (see inset on Figure 11). We interpret that these graben form as a consequence of the fault trying to reduce throw and terminate, in the presence of a barrier to further lateral propagation. In addition, stress perturbations proximal to the margin of the granitic TBF Footwall Block may have locally influenced the rotated WNW-ESE striking faults (Figure 11) (cf. Morley 2010; Rotevatn et al. 2018b). Some NE-trending faults are identified to the south west of the horsetail splay faults (i.e. Faults 17 and 20 in Figure 11), forming E-W to NE-SW trending grabens. We suggest that these relatively low-displacement faults broke through the initial barrier to propagation following an initial period of retardation at the TBF Footwall Block (Figure 11).

5.3 Reactivation of basement fabrics

We identify two prominent basement fabrics across the Great South Basin, dipping towards the south (Figure 12) and to the east (Figure 13). These fabrics are also associated with faults that offset the top Acoustic Basement horizon and align with the fabric in basement (Figure 12, 13). The fabrics are characterised by relatively linear dipping packages of reflections within basement, often truncated at a high angle by the top Acoustic Basement surface. The fabrics often mutually cross-cut oppositely-dipping basement reflections and display small-scale (~1 km wide), high-amplitude reflections in these areas (Figure 12, 13). Additional basement reflectivity, associated with the Terrane Boundary shear zone and the granitic body, is also present throughout the area but is distinct from these basement fabrics (Figure 12).

The basement fabrics are developed throughout the study area but are most pronounced across the granitic footwall block of the Terrane Boundary Fault, where they are shown to be associated with an E-W trending and a NE-SW trending fault population across the Acoustic Basement surface (Figure 14). At first glance, the different fabrics appear to display mutually cross-cutting relationships, with no ability to distinguish relative timing of formation (Figure 5, 6). However, the NE-SW fabric appears to offset the E-W fabric in some areas; in addition, the NE-SW fabric also appears to abut against the fabric rather than be offset by it (Figure 14), although this relationship is not clear. However, in cross-section, we observe that the fabrics associated with the NE-trending faults offset the E-W striking fabrics associated with the shear zone (Figure 7), indicating that the NE-SW fabric postdates the E-W fabric (Figure 14).

The E-W fabric aligns with and shares a similar S-dipping geometry as the Terrane Boundary Fault and shear zone. This fabric does not appear to be related to the NE-trending faults within the basin, including the Splaying Fault system, which cross-cut the fabric (Figure 12). The NE-SW fabric is aligned with, and displays a similar dip to, the NE-trending fault population.

Prominent fabrics as observed on seismic reflection data may be related to a number of different features including sedimentary strata, fault plane reflections, highly foliated basement rocks and shear zones (Phillips et al. 2016; Fazlikhani et al. 2017; Lenhart et al. 2019) and dyke swarms (Abdelmalak et al. 2015; Phillips et al. 2017). The E-W fabric appears to be associated with the Terrane Boundary Fault and associated shear zone, appearing to link with the structure to the south (Figure 12). This fabric may therefore represent shear-related fabrics within the granitic block, exploited by multiple low-displacement faults. This generation of this fabric may relate to an early phase of activity within the Great South Basin, potentially related to the early stages of the separation of Zealandia and Australia (Kula et al. 2007; Tulloch et al. 2019), or extension within a back-arc setting (Uruski 2010).

The NE-SW fabric appears to be related to NE-trending faults formed due to NW-SE oriented extension associated with formation of the Great South Basin and the separation of Zealandia and Western Antarctica (Kula et al. 2007; Sahoo et al. 2014; Tulloch et al. 2019). Faults associated with this extension are proposed to link to a detachment at mid-crustal depths (Uruski et al. 2007). We suggest that this fabric may relate to hangingwall flexure associated with this activity. Alternatively, in some areas the fabric may also represent the rotated sedimentary bedding-related reflectivity from an earlier rift phase. Although this doesn’t match the with the relationship between the main E-dipping fabric and faults shown in Figure 13, it may be associated with a fault out of the plane of the section. In this instance, the rotated bedding-related reflectivity may be exploited by faults during later hangingwall flexure (Figure 13).

6. Discussion

6.1 Terrane boundary reactivation and the regional evolution of the Great South Basin

The Great South Basin formed perpendicular to the boundaries between a series of basement terranes accreted along the southern margin of Gondwana during a protracted period of subsidence (Beggs

1993; Mortimer et al. 2002). Following Cenozoic-to-recent activity along the Alpine Fault (Cooper et al. 1987; Cooper & Norris 1994; Sutherland et al. 2000), the terranes underlying the Great South Basin are also present offshore North Island, beneath the Taranaki Basin (Muir et al. 2000; Collanega et al. 2018). Regional seismic data indicates that the boundaries between individual terranes extend throughout the crust, and likely the lithosphere (Muir et al. 2000; Mortimer et al. 2002).

We identified in this study a major crustal-scale shear zone and associated upper-crustal fault system between the Median Batholith and Western Province terranes, representing a reactivation of the terrane boundary (Figure 5, 6). To the north, in the Taranaki Basin, the boundary between these terranes was initially exploited by the intrusion of the Separation Point Batholith suite, with the Cape Egmont Fault zone then exploiting the boundary between the Separation Point and Median batholiths (Muir et al. 2000; Collanega et al. 2018). In this instance, the terrane boundary appears to have also been initially exploited by granitic bodies belonging to the Separation Point Batholith suite, as also sampled along strike in the Pukaki-1 well. Subsequently, this terrane boundary is later reactivated, with the formation of a shear zone along the margin of the granite (Figure 15, 16). The localisation of the shear zone along the margin of the granitic body may explain why the shear zone thins with depth. At deeper levels the shear zone is pinned along the margin of the granite, whereas at shallower basement levels, where the granite may be absent, the shear zone is less confined. The prominent contrast in lithological properties between the Median Batholith, including the Separation Point Batholith suite, and the Western Province terranes localised strain and led to reactivation of the terrane boundary (Figure 15).

The WNW-trending Terrane Boundary Fault is oriented at a high angle to the NE-trending faults of the Great South Basin (Figure 1). Whilst it is possible that local stress perturbations relating to pre-existing structures led to the development of non-optimally oriented structures (Morley 2010; Philippon et al. 2015; Phillips et al. 2016; Rotevatn et al. 2018b; Samsu et al. 2019), we do not think that this is the case due to the high angle between the structures. Instead, we propose that these non-collinear structures formed during multiple phases of extension relating to the multiphase breakup of Gondwana in the Late Cretaceous (Kula et al. 2007; Tulloch et al. 2019). Based on geometric relationships between the NE- and E- basement fabrics (Figure 7, 14, 15c), we suggest that the WNW-trending structures formed prior to the NE-trending faults and fabrics. An initial phase of extension occurred at 100-90 Ma, related to the breakup between Australia and the contiguous Zealandia and Western Antarctica. Offshore of the southeast South Island, the extension direction was oriented roughly NE-SW (Tulloch et al. 2019), with the boundaries between basement terranes, representing crustal-scale weaknesses that were optimally oriented to be reactivated during this phase of extension. We suggest that this initial phase of extension was responsible for the formation of the Terrane boundary shear zone and associated fault. This phase of activity was also associated with activity across the Sisters Shear Zone, onshore Stewart Island (Kula et al. 2009). Although the WNW-trending Terrane Boundary shear zone is oblique to the NE-trending Sisters Shear Zone, it is aligned with the Gutter Shear zone and the Freshwater and Escarpment fault systems, which show dextral transpressional activity during the Early Cretaceous (Allibone & Tulloch 2004, 2008). While some oblique slip is possible along the Terrane Boundary Fault, this would not appear to be the case based on the SSW-directed transport of footwall blocks and the orientation of the embayments (Figure 4, 7). Therefore, we suggest that the geometry of the Terrane Boundary Shear zone was controlled by the granite body, and therefore not aligned with the Sisters shear zone.

Following breakup between Australia and Zealandia, a second phase of rifting occurred from ~90-80 Ma and was related to the breakup of Zealandia and Western Antarctica, leaving Zealandia as an isolated continent. This phase of extension was oriented NW-SE and resulted in the formation of NE-trending faults across the Great South Basin and thinning of the crustal thickness to ~22 km (Beggs 1993; Uruski et al. 2007; Grobys et al. 2009; Sahoo et al. 2014). This phase of activity was oriented at a high angle to the WNW-trending Terrane boundary, which was therefore not reactivated. However, the Terrane boundary shear zone, and the granitic body in its immediate footwall, blocked the lateral propagation of faults and segmented the rift (Figure 15b) (Dore et al. 1997; Corti 2008; Koopmann et al. 2014; Henstra et al. 2015; Peace et al. 2017; Heilman et al. 2019).

6.2 3D geometry and seismic expression of a granitic batholith

Although the Median Batholith represents a large area of igneous material, it is by no means a homogeneous body. The batholith is a composite structure formed during a protracted period of magmatism and comprises multiple generations of plutonic material with complex overprinting relationships as observed onshore (Mortimer et al. 1999; Allibone & Tulloch 2004). The large, composite nature of the Median Batholith resembles other batholiths worldwide, such as the Cordillera Blanca batholith of the Peruvian Andes (Petford & Atherton 1992) and the North American Sierra Nevada Batholith (Schwartz et al. 2014).

We suggest the granitic body underpinning the TBF Footwall Block belongs to the Cretaceous-aged Separation Point Batholith Suite. Intrusions displaying Separation Point affinity have been identified along the same terrane boundary in the Taranaki Basin (Mortimer et al. 1997; Muir et al. 2000), and form the basement of the Pukaki-1 well, which is also situated along the footwall of the Terrane Boundary Fault (Figure 1) (Tulloch et al. 2019). Late Early Cretaceous batholiths along-strike to the northwest on Stewart Island are largely confined to the south of the Gutter Shear zone, towards the boundary with the Western Province terranes (Mortimer et al. 1999; Allibone & Tulloch 2004). The Separation Point suite was intruded into Carboniferous-aged plutons, such as those penetrated in the Pakaha-1 well (Figure 1) (Tulloch et al. 2019). The spatial relationships between the granitic bodies offshore resembles those observed onshore Stewart Island (Allibone & Tulloch 2004).

Due to their relatively homogeneous nature, granitic bodies do not generate prominent impedance contrasts and often appear acoustically transparent on seismic reflection data. However, reflections can be generated at contacts between the granitic body and surrounding country rock, giving us insights into the gross granite morphology. Seismic reflections have previously been identified originating from the top and base of granitic bodies (Lynn et al. 1981; McLean et al. 2017; Howell et al. 2019), as well as from internal fractures (Mair & Green 1981) and layered granitic laccoliths (Evans et al. 1993; Evans et al. 1994). When observed in seismic data, granitic intrusions typically display a laccolith-style geometry, consisting of stacked, lenticular bodies (Lynn et al. 1981; Evans et al. 1994; McCaffrey & Petford 1997; Petford et al. 2000). Beneath the TBF Footwall Block, we observe layered and domal packages of reflections, resembling laccolith style geometries (Figure 5, 6, 15a), whereas across the TBF Footwall Block itself we identify some areas displaying relatively acoustically transparent seismic facies (Figure 12, 13). These acoustically transparent areas in some places may be cross-cut by shear zone-related reflectivity, potentially corresponding to faults and fractures within the granite itself (Figure 12).

The geometry of the interpreted granite body shows some variability along-strike and is not at a constant depth beneath the top Acoustic Basement surface (cf. Howell et al. 2019). In the west, the granite displays a laccolith style geometry and extends up to ~3 s TWT (Figure 5). In the east, it displays a more domal geometry that extends up to ~5 s TWT, and stops at greater depths beneath the Acoustic Basement (Figure 6). Relief on the top surface of granitic bodies has also been identified in the Lake District and North Pennine batholiths onshore UK (Howell et al. 2019). We propose that the relief atop the granite and its depth beneath the top Acoustic Basement surface is expressed in the rift physiography, controlling the location of embayments along the footwall of the Terrane Boundary Fault (Figure 16). In areas where the granitic body extends to shallow depths beneath the top Acoustic Basement surface, we identify a steep shear zone with a series of fault blocks detaching along its margin (Figure 5, 16). However, where the granite sits at greater depths beneath the top Acoustic Basement surface, the upper part of the shear zone rotates to shallower dips across the top of the granite and incises backwards into the TBF Footwall Block, creating embayments that contain 'perched' fault blocks atop a sub-horizontal detachment (Figure 6, 16). This indicates that the shallow relatively unfaulted areas of the TBF Footwall Block represent areas where the granite reaches shallow depths within basement and that the overall physiography of the TBF Footwall Block may act as a proxy for that of the underlying granite (Figure 4a, 16).

The granite-cored TBF Footwall Block is relatively unfaulted and forms a structural high relative to adjacent areas. Furthermore, the areas where the granite is located at shallow depths form further relative highs within the TBF Footwall Block (Figure 4). Granitic bodies often form the core to basement structural highs such as the Utsira High in the North Sea (Slagstad et al. 2011; Lundmark et al. 2013); the Alston Block in the UK (Critchley 1984; Howell et al. 2019) and the Sierra Nevada Batholith in the USA (Ducea & Saleeby 1996; Van Buer et al. 2009). Previous studies have proposed that the reduced density and increased rigidity of granite compared to adjacent basement rocks makes them less susceptible to rifting when exposed to extensional stresses (Bott et al. 1958; de Castro et al. 2007). Whilst this increased buoyancy plays an important role in the formation of granite-cored structural highs, isostatic forces relating to initial granite emplacement also play an important role (Howell et al. 2019). These granitic bodies show a partitioning of strain and deformation around their margins rather than internally. One potential mechanism for the lack of faulting across granite-cored structural highs may be the absence of prominent heterogeneities within these relatively homogeneous bodies upon which strain can initially localise (Mair & Green 1981; Howell et al. 2019).

6.3 Strain accommodation along a laterally inhibited fault system

The Splaying Fault System segments as it approaches the granite-cored TBF Footwall Block (Figure 4). Cumulative fault throw remains relatively constant across the system as it approaches the block, with a large displacement gradient present at the boundary with the block itself (Figure 9, 10). The relatively constant cumulative throw along the fault indicates a large degree of kinematic coherence within the system, with individual fault segments behaving as a singular system (Walsh & Watterson 1991; Walsh et al. 2002; Walsh et al. 2003; Childs et al. 2017; Jackson et al. 2017; Rotevatn et al. 2018a). In cross-section, some faults also appear linked at depth, forming a single structure indicative of a degree of geometric coherence (Figure 8) (Walsh & Watterson 1991; Walsh et al. 2003; Giba et al. 2012; Jackson et al. 2017). However, the NW-dipping fault segments splaying from the footwall block of the main structure display kinematic coherence with the main system but are not geometrically linked (Figure 8).

Although a steep gradient is present for cumulative throw on the Splaying Fault System at the boundary with the TBF Footwall Block, such a gradient is not apparent for the individual segments themselves, which display more typical throw profiles (Figure 9, 10) (Childs et al. 2017). As the Splaying Fault System approaches this mechanically stronger barrier to lateral fault propagation, it splays into a series of lower displacement segments. These segments display lower throw gradients and are able to terminate easier than a single large structure (Figure 15b). Similar splaying fault geometries are present at fault terminations across all scales. Deformation along the Alpine Fault is accommodated by splays of the Marlborough fault system to the northwest, where it starts to interact with the Hikurangi subduction zone (Norris & Cooper 2001; Wannamaker et al. 2009). The eastern branch of the East African Rift forms a series of rift segments to the south, termed the North Tanzania Divergence Zone, where strain is accommodated over a wider area as rifting propagates toward and eventually terminates in the cratonic lithosphere of the Tanzania Craton (Ebinger et al. 1997; Foster et al. 1997; Ring et al. 2005). At smaller scales, geometrically similar structures, such as horsetail splays and damage zones are commonly associated with the lateral terminations of fault systems (Kim & Sanderson 2006; Mouslopoulou et al. 2007; Perrin et al. 2016; Nicol et al. 2017).

A key question remains whether the fault propagated towards the footwall block or whether the system formed geologically instantaneously (i.e. following the constant length fault model) (Walsh et al. 2002; Childs et al. 2017; Nicol et al. 2017) but displayed different structural styles along its length. Furthermore, it is also unclear why the fault splayed at this particular location, outboard of the TBF Footwall Block, rather than at the boundary. Nixon et al. (2014) document a transition from localised to distributed extension within a kinematically coherent fault system in the Whakatane Graben, which they link to progressive strain localisation along the system. However, the segmentation in this instance occurs over a relatively short distance and does not resemble the gradual increase in segmentation, and the area over which strain is accommodated, observed in the Great South Basin (Figure 4, 15b). If the entire fault length did form geologically instantaneously, rather than propagate to the southwest, why the fault changed structural style in that specific location would still require an explanation, as the boundary with the TBF Footwall Block is located further to the southwest, with no major change in underlying structure at the point of initial splaying. Damage zones relating to granite emplacement may have locally altered lithological properties of basement rocks; however, this would only affect a limited area. In addition, local rotation and alignment of fault segments are only identified along the margin of the TBF Footwall Block (Figure 4, 11), and are not present where the fault begins to splay. Based on the gradational splaying of the fault system and the apparent lack of change in basement physiography at the initial site of segmentation, we suggest that the fault propagated towards the granite block, although the timescale of this propagation is shorter than the temporal resolution provided by our seismic data.

As the faults rotate at the margin of the TBF Footwall Block, they appear to detach onto the granite (Figure 3, 8d), implying that the northern margin of the granite dips northwards. One possibility for why the fault splays where it does is that the dipping margin of the stronger granitic block restricts the maximum fault height, such that where the faults interact with the granite boundary at depth is offset from the boundary at the surface (Figure 15b). The initial site of fault splaying may correspond to the area where the deeper levels of the fault start to interact with the granite body. As the fault approaches, its maximum height is reduced, causing the fault to splay into multiple segments (Figure 15b). This could potentially explain the splaying of the fault system, although we are unable to determine this scenario in our data.

As previously stated, individual fault segments rotate along the margin of the TBF Footwall Block (Figure 11, 15b). This may be related to local stress perturbations along the margin of the block (Morley 2010; Philippon et al. 2015; Morley 2017; Rotevatn et al. 2018b), or alternatively to a change in structural style along the faults from dip- to strike-slip (Mouslopoulou et al. 2007). The horsetail splay geometries identified across the intra-Upper Cretaceous surface (Figure 11) describe two WNW-trending grabens, which would not appear to fit with strike-slip motion. However, these grabens are not present at the top Acoustic Basement horizon and the individual faults may link together at depth, indicating that they could be related to oblique activity on a deeper fault. However, in other areas faults align along the margin of the TBF Footwall Block and show no evidence of strike-slip activity (Figure 4b). These faults appear to detach onto the north dipping northern margin of the granite, showing similar relationships to those along the Pakaha ridge (Figure 3, 8d). The rooting of faults onto the granitic body may also explain the switch in polarity along the Splaying Fault System, from SE-dipping in the northeast, to NW-dipping further southwest. In the southwest, the NW-dipping faults appear to detach onto the granite at depth, preferentially exploiting this pre-existing heterogeneity (Figure 8d).

7. Conclusions

In this study, we have analysed the detailed structural evolution of the southern section of the Great South Basin and examined how it has been influenced by various structural heterogeneities relating to the underlying Median Batholith Zone. We have documented a range of styles of structural inheritance, which exert variable influences over rift physiography throughout multiple tectonic events. We find that:

- The offshore extension of the terrane boundary between the Median Batholith Zone and Western Province terranes, trends WNW across the Great South Basin. This terrane boundary is associated with a crustal-to-lithospheric scale shear zone and is associated with a series of faults in the upper crust that segment the Great South Basin. Reactivation of the terrane boundary occurred in response to NE-SW oriented extension related to the separation of Australia and New Zealand.
- We postulate a granite cored structural high resides in the footwall of the reactivated terrane boundary. Based on seismic interpretation, regional context and nearby well information, we interpret that the granitic body displays a laccolith-style geometry and is part of the Cretaceous Separation Point Batholith suite. This batholith suite may have exploited the original lithosphere-scale terrane boundary along the southern margin of the Median Batholith and later appeared to localise the shear zone along its southern margin.
- We infer details of the 3D geometry of the granitic body from the overlying rift physiography. Where the granite reaches shallow depths, it controls the shallow geometry of the Terrane Boundary shear zone, which tracks along the granite margin and is associated with hangingwall fault blocks; where the granite top sits at greater depths, the shear zone shallows atop the granite and forms shallow embayments that incise into the footwall. These features act as a proxy for the relief of the top of the granite body.
- The granite-cored basement high acts as a barrier to the lateral propagation of NE-trending faults within the Median Batholith. These faults form a series of splays that eventually rotate

into parallelism as they approach the mechanically strong granite body, with relatively few faults present across the high itself. NE-trending faults formed in response to NW-SE directed extension related to the separation and breakup of New Zealand and West Antarctica.

- Individual segments within the splaying fault system display kinematic and geometric coherence along the fault system and accommodate similar values of extension along-strike. The initial site of splaying along the fault system is offset from the granite boundary, perhaps relating to a N-dipping granite margin.
- Two generations of basement fabrics are developed across the basin, trending E-W and NE-SW. These fabrics are proposed to be related to the reactivation of the terrane boundary and the NW-SE directed rifting respectively. They are exploited by numerous small, low-displacement faults, which are particularly well developed atop the granite-cored basement high.

Acknowledgements

This work is funded by the Leverhulme Trust in the form of a Leverhulme Early Career Fellowship awarded to Phillips. We would like to thank New Zealand Petroleum and Minerals for making the seismic data used in this study publically available. We would also like to thank Schlumberger for providing academic licences to the University of Durham for the use of Petrel software.

Figure captions

***Figure 1* –** Map showing the top Acoustic Basement structure surface (in two way travel time – TWT) across the study area of the Great South Basin in relation to the underlying basement terranes. Terrane boundaries after Ghisetti (2010) and Mortimer et al. (2002). NE-trending faults are present throughout the basin, with a large WNW-trending fault present along its southern margin. Inset – regional map of New Zealand showing basement terranes offset along the Alpine Fault. Also shown are the locations

of the Great South and Canterbury basins offshore the South Island, as well as bathymetric features including the Campbell Plateau, Chatham Rise and Bounty Trough.

Figure 2 – Stratigraphic column showing international and New Zealand stratigraphic ages for a series of prominent stratigraphic horizons and lithologies mapped throughout the basin. Stratigraphic horizons are tied to the Pukaki-1 well.

Figure 3 – Uninterpreted and interpreted E-W oriented seismic section across the centre of the Great South Basin. See Figure 1 for location. Key stratigraphic horizons are linked to the Pakaha-1 well. Faults along the southwestern margin of the basin merge along the margin of the granitic Pakaha ridge. A complex series of cross-cutting faults are present in the centre of the basin.

Figure 4 – A) TWT structure map of the top Acoustic Basement surface based on 3D seismic volume across the centre of the basin, see Figure 1 for location. The basin is dominated by NE-trending faults with the SSW-dipping Terrane Boundary Fault along the southern margin of the basin. A WNW-trending, relatively unfaulted structural high is located in the footwall of the Terrane Boundary Fault, termed the TBF Footwall Block. B) TWT structure map of a key surface within the Upper Cretaceous interval (see Figure 3). A SE-dipping fault becomes segmented towards the southwest and forms a series of splays as it approaches the TBF Footwall Block.

Figure 5 – Uninterpreted and interpreted N-S oriented seismic section across the western platform of the study area. See Figure 1 for location. The boundary between the Median Batholith and Western Province terranes is marked by the blue line. Divergent syn-rift strata are marked by dark green wedges. A large shear zone is co-located with the boundary between the terranes.

Figure 6 – uninterpreted and interpreted N-S oriented seismic section across the centre of the study area. See Figure 1 for location. Boundary between the Median Batholith and Western Province terranes is marked by the blue line and is associated with a shear zone and fault system, termed the Terrane Boundary Fault. A large area of complex faulting is present in the footwall of the Terrane Boundary Fault.

***Figure 7* –** uninterpreted and interpreted N-S oriented seismic section across the TBF Footwall Block and a prominent footwall embayment. See Figure 4 for location. Basement reflectivity is shown associated with the Terrane Boundary Shear Zone and is cross-cut by fabrics associated with NE-trending faults.

***Figure 8* –** Uninterpreted and interpreted seismic sections along-strike of the Splaying Fault System. See Figure 4 for locations. A) Section across the northeastern extent of the Splaying Fault System, where strain is accommodated by a single fault. Sub-Acoustic Basement reflectivity is present, likely relating to an earlier phase of activity of undetermined age. B) Towards the southwest the fault begins to splay into a series of segments. Synthetic fault segments form in response to dissection of the footwall as antithetic faults form in the hangingwall and merge with the main fault plane. C) The footwall of the fault is now highly deformed with extension accommodated by a wide zone of deformation consisting of SE- and NW-dipping faults. D) Extension is accommodated by a wide zone of deformation, with the dominant faults now dipping to the NW and detaching onto the margin of a granitic ridge. Rotation of the faults to a WNW-ESE strike is accommodated by the formation of shallow synthetic and antithetic faults in the footwall and hangingwall of the faults respectively.

***Figure 9* –** Throw-length profiles calculated across the Acoustic Basement surface for individual segments of the Splaying Fault System. Individual profiles are colour-coded to the faults on the surface to the right. Also shown is the cumulative throw across the whole of the system, calculated by summing throw on individual segments across a lines perpendicular to the strike projection of the main fault. Also shown are the locations of the sections shown in Figure 8.

***Figure 10* –** Throw-length profiles calculated across the intra-Upper Cretaceous surface for individual segments of the Splaying Fault System as well as the cumulative throw across the system. Fault colours are coded to the surface on the right, but are not related to those shown in Figure 9. Note that the cumulative throw is relatively consistent across the system regardless of the degree of segmentation, before a steep displacement gradient towards the boundary of the TBF Footwall Block.

Figure 11 – Uninterpreted TWT structure map and detailed interpretations of horsetail-splay style fault geometries across the Intra-Upper Cretaceous surface. See Figure 4b for location. Fault numbers refer to those in Figure 10. Inset – Two seismic sections across the area corresponding to the blue and purple lines on the figure.

Figure 12 – Uninterpreted and interpreted NNE-SSW oriented seismic sections across the TBF Footwall Block, highlighting the E-W oriented basement fabrics. See Figures 4 and 14 for location. Shear-zone related reflectivity is shown by the thick dashed black lines, whilst the basement fabrics are represented by the dark blue lines. NE-trending faults post-date and cross-cut the shear zone related reflectivity.

Figure 13 – Uninterpreted and interpreted E-W oriented seismic section across the TBF Footwall Block, highlighting the NE-trending basement fabric. See Figures and 14 for location. The basement fabric displays a similar dip to the NE-trending faults and is often associated with low-displacement faults across the top Acoustic Basement surface.

Figure 14 – TWT structure map showing E-W and NE-SW oriented faults associated with underlying fabrics across the top Acoustic Basement surface. See Figure 4a for location. Abutting and potentially cross-cutting relationships are observed between the different generations of faults, although no clear relative age relationships can be identified.

Figure 15 – Schematic cartoons showing the different styles of structural inheritance identified in the Great South Basin across different scales. A) Shear zone and associated fault localise along the Terrane boundary and the margin of the continuation of the Separation Point Batholith Suite between the Median Batholith and Western Province. Inset shows the localisation of the shear zone along the granite margin. B) The stronger material in the footwall to the Terrane Boundary Fault forms a barrier to lateral fault propagation, causing faults to splay as they approach and strain to be accommodated across multiple low-displacement segments. Inset – The dipping boundary of the strong barrier restricts fault height away from the boundary at the surface, causing the initial site of fault splaying to be offset from the boundary at shallower depths. C) Exploitation of prominent basement fabrics by

relatively low-displacement faults. Differently oriented fabrics may be exploited at different times and during different tectonic events, resulting in multiple generations of faults. Inset – Cross-sectional view showing the reactivation and cross-cutting relationships between different fabrics.

Figure 16 **–** 3D model showing the relationship between the Terrane Boundary Shear Zone and the relief of the top of the granitic body. The shear zone localises along the margin of the granite body. Where the granitic is situated at shallower depths the shear zone tracks along the margin and is associated with a series of detaching fault blocks; where the shear zone is situated at greater depths, it shallows atop the granite and forms embayments that cut back into the footwall.

References

Abdelmalak, M.M., Andersen, T.B., Planke, S., Faleide, J.I., Corfu, F., Tegner, C., Shephard, G.E., Zastrozhnov, D., *et al.* 2015. The ocean-continent transition in the mid-Norwegian margin: Insight from seismic data and an onshore Caledonian field analogue. *Geology*, **43**, 1011-1014, http://doi.org/10.1130/G37086.1.

Allibone, A.H. & Tulloch, A.J. 2004. Geology of the plutonic basement rocks of Stewart Island, New Zealand. *New Zealand Journal of Geology and Geophysics*, **47**, 233-256, http://doi.org/10.1080/00288306.2004.9515051.

Allibone, A.H. & Tulloch, A.J. 2008. Early Cretaceous dextral transpressional deformation within the Median Batholith, Stewart Island, New Zealand. *New Zealand Journal of Geology and Geophysics*, **51**, 115-134, http://doi.org/10.1080/00288300809509854.

Bache, F., Sutherland, R., Stagpoole, V., Herzer, R., Collot, J. & Rouillard, P. 2012. Stratigraphy of the southern Norfolk Ridge and the Reinga Basin: A record of initiation of Tonga–Kermadec–Northland subduction in the southwest Pacific. *Earth and Planetary Science Letters*, **321-322**, 41-53, http://doi.org/https://doi.org/10.1016/j.epsl.2011.12.041.

Bache, F., Mortimer, N., Sutherland, R., Collot, J., Rouillard, P., Stagpoole, V. & Nicol, A. 2014. Seismic stratigraphic record of transition from Mesozoic subduction to continental breakup in the Zealandia sector of eastern Gondwana. *Gondwana Research*, **26**, 1060-1078, http://doi.org/https://doi.org/10.1016/j.gr.2013.08.012.

Beggs, J. 1993. Depositional and tectonic history of the Great South Basin. *South Pacific sedimentary basins. Sedimentary basins of the World*, **2**, 365-373.

Bishop, D., Bradshaw, J. & Landis, C. 1985. Provisional terrane map of South Island, New Zealand.

Bott, M.H.P., Day, A.A. & Massonsmith, D. 1958. The Geological Interpretation of Gravity and Magnetic Surveys in Devon and Cornwall. *Philosophical Transactions of the Royal Society of London Series a-Mathematical and Physical Sciences*, **251**, 161-191, http://doi.org/10.1098/rsta.1958.0013.

Bradshaw, J.D. 1989. Cretaceous Geotectonic Patterns in the New-Zealand Region. *Tectonics*, **8**, 803-820, http://doi.org/10.1029/TC008i004p00803.

Campbell, H.J., Mortimer, N. & Turnbull, I.M. 2003. Murihiku Supergroup, New Zealand: Redefined. *Journal of the Royal Society of New Zealand*, **33**, 85-95, http://doi.org/10.1080/03014223.2003.9517722.

Carreras, J. 2001. Zooming on Northern Cap de Creus shear zones. *Journal of Structural Geology*, **23**, 1457-1486, http://doi.org/https://doi.org/10.1016/S0191-8141(01)00011-6.

Chattopadhyay, A. & Chakra, M. 2013. Influence of pre-existing pervasive fabrics on fault patterns during orthogonal and oblique rifting: An experimental approach. *Marine and Petroleum Geology*, **39**, 74-91, http://doi.org/http://dx.doi.org/10.1016/j.marpetgeo.2012.09.009.

Childs, C., Holdsworth, R.E., Jackson, C.A.L., Manzocchi, T., Walsh, J.J. & Yielding, G. 2017. Introduction to the geometry and growth of normal faults. *Geological Society, London, Special Publications*, **439**, 1, http://doi.org/10.1144/SP439.24.

Coleman, A.J., Jackson, C.A.L., Nikolinakou, M.A. & Duffy, O.B. 2018. How, where, and when do radial faults grow near salt diapirs? *Geology*, **46**, 655-658, http://doi.org/10.1130/G40338.1.

Collanega, L., Jackson, C.A.L., Bell, R.E., Coleman, A.J., Lenhart, A. & Breda, A. 2018. Normal fault growth influenced by basement fabrics: the importance of preferential nucleation from pre-existing structures. *Basin Research*, **0**, http://doi.org/10.1111/bre.12327.

Cooper, A.F. & Norris, R.J. 1994. Anatomy, structural evolution, and slip rate of a plate-boundary thrust: The Alpine fault at Gaunt Creek, Westland, New Zealand. *GSA Bulletin*, **106**, 627-633, http://doi.org/10.1130/0016-7606(1994)106<0627:ASEASR>2.3.CO;2.

Cooper, A.F., Barreiro, B.A., Kimbrough, D.L. & Mattinson, J.M. 1987. Lamprophyre dike intrusion and the age of the Alpine fault, New Zealand. *Geology*, **15**, 941-944, http://doi.org/10.1130/0091-7613(1987)15<941:LDIATA>2.0.CO;2.

Corti, G. 2008. Control of rift obliquity on the evolution and segmentation of the main Ethiopian rift. *Nature Geoscience*, **1**, 258, http://doi.org/10.1038/ngeo160 https://www.nature.com/articles/ngeo160#supplementary-information.

Critchley, M.F. 1984. Variscan tectonics of the Alston block, northern England. *Geological Society, London, Special Publications*, **14**, 139, http://doi.org/10.1144/GSL.SP.1984.014.01.14.

Daly, M.C., Chorowicz, J. & Fairhead, J.D. 1989. Rift basin evolution in Africa: the influence of reactivated steep basement shear zones. *Geological Society, London, Special Publications*, **44**, 309, http://doi.org/10.1144/GSL.SP.1989.044.01.17.

Davy, B., Hoernle, K. & Werner, R. 2008. Hikurangi Plateau: Crustal structure, rifted formation, and Gondwana subduction history. *Geochemistry, Geophysics, Geosystems*, **9**, http://doi.org/10.1029/2007GC001855.

Dawson, S.M., Laó-Dávila, D.A., Atekwana, E.A. & Abdelsalam, M.G. 2018. The influence of the Precambrian Mughese Shear Zone structures on strain accommodation in the northern Malawi Rift. *Tectonophysics*, **722**, 53-68, http://doi.org/https://doi.org/10.1016/j.tecto.2017.10.010.

de Castro, D.L., de Oliveira, D.C. & Gomes Castelo Branco, R.M. 2007. On the tectonics of the Neocomian Rio do Peixe Rift Basin, NE Brazil: Lessons from gravity, magnetics, and radiometric data. *Journal of South American Earth Sciences*, **24**, 184-202, http://doi.org/https://doi.org/10.1016/j.jsames.2007.04.001.

De Paola, N., Holdsworth, R.E. & McCaffrey, K.J.W. 2005. The influence of lithology and pre-existing structures on reservoir-scale faulting patterns in transtensional rift zones. *Journal of the Geological Society*, **162**, 471, http://doi.org/10.1144/0016-764904-043.

Dichiarante, A.M., Holdsworth, R.E., Dempsey, E.D., Selby, D., McCaffrey, K.J.W., Michie, U.M., Morgan, G. & Bonniface, J. 2016. New structural and Re–Os geochronological evidence constraining the age of faulting and associated mineralization in the Devonian Orcadian Basin, Scotland. *Journal of the Geological Society*, **173**, 457, http://doi.org/10.1144/jgs2015-118.

Dore, A.G., Lundin, E.R., Fichler, C. & Olesen, O. 1997. Patterns of basement structure and reactivation along the NE Atlantic margin. *Journal of the Geological Society*, **154**, 85-92, http://doi.org/DOI 10.1144/gsjgs.154.1.0085.

Ducea, M.N. & Saleeby, J.B. 1996. Buoyancy sources for a large, unrooted mountain range, the Sierra Nevada, California: Evidence from xenolith thermobarometry. *Journal of Geophysical Research-Solid Earth*, **101**, 8229-8244, http://doi.org/10.1029/95jb03452.

Duffy, O.B., Bell, R.E., Jackson, C.A.L., Gawthorpe, R.L. & Whipp, P.S. 2015. Fault growth and interactions in a multiphase rift fault network: Horda Platform, Norwegian North Sea. *Journal of Structural Geology*, **80**, 99-119, http://doi.org/http://dx.doi.org/10.1016/j.jsg.2015.08.015.

Ebinger, C., Djomani, Y.P., Mbede, E., Foster, A. & Dawson, J.B. 1997. Rifting Archaean lithosphere: the Eyasi-Manyara-Natron rifts, East Africa. *Journal of the Geological Society*, **154**, 947, http://doi.org/10.1144/gsjgs.154.6.0947.

Evans, D.J., Rowley, W.J., Chadwick, R.A. & Millward, D. 1993. Seismic reflections from within the Lake District batholith, Cumbria, northern England. *Journal of the Geological Society*, **150**, 1043, http://doi.org/10.1144/gsjgs.150.6.1043.

Evans, D.J., Rowley, W.J., Chadwick, R.A., Kimbell, G.S. & Millward, D. 1994. Seismic reflection data and the internal structure of the Lake District batholith, Cumbria, northern England. *Proceedings of the Yorkshire Geological and Polytechnic Society*, **50**, 11, http://doi.org/10.1144/pygs.50.1.11.

Fazlikhani, H., Fossen, H., Gawthorpe, R., Faleide, J.I. & Bell, R.E. 2017. Basement structure and its influence on the structural configuration of the northern North Sea rift. *Tectonics*, **36**, 1151-1177, http://doi.org/10.1002/2017tc004514.

Fossen, H., Khani, H.F., Faleide, J.I., Ksienzyk, A.K. & Dunlap, W.J. 2016. Post-Caledonian extension in the West Norway–northern North Sea region: the role of structural inheritance. *Geological Society, London, Special Publications*, **439**, http://doi.org/https://doi.org/10.1144/SP439.6.

Foster, A., Ebinger, C., Mbede, E. & Rex, D. 1997. Tectonic development of the northern Tanzanian sector of the East African Rift System. *Journal of the Geological Society*, **154**, 689, http://doi.org/10.1144/gsjgs.154.4.0689.

Freeman, B., Klemperer, S.L. & Hobbs, R.W. 1988. The deep structure of northern England and the Iapetus Suture zone from BIRPS deep seismic reflection profiles. *Journal of the Geological Society*, **145**, 727, http://doi.org/10.1144/gsjgs.145.5.0727.

Ghisetti, F. 2010. Seismic interpretation, Propsects and Strucutral Analysis, Great South Basin. Ministry of Economic Development New Zealand Unpublished Petroleum Report PR4173.

Giba, M., Walsh, J.J. & Nicol, A. 2012. Segmentation and growth of an obliquely reactivated normal fault. *Journal of Structural Geology*, **39**, 253-267, http://doi.org/10.1016/j.jsg.2012.01.004.

Grobys, J.W.G., Gohl, K., Uenzelmann-Neben, G., Davy, B. & Barker, D. 2009. Extensional and magmatic nature of the Campbell Plateau and Great South Basin from deep crustal studies. *Tectonophysics*, **472**, 213-225, http://doi.org/https://doi.org/10.1016/j.tecto.2008.05.003.

Grobys, J.W.G., Gohl, K., Davy, B., Uenzelmann-Neben, G., Deen, T. & Barker, D. 2007. Is the Bounty Trough off eastern New Zealand an aborted rift? *Journal of Geophysical Research: Solid Earth*, **112**, http://doi.org/10.1029/2005JB004229.

Hedin, P., Almqvist, B., Berthet, T., Juhlin, C., Buske, S., Simon, H., Giese, R., Krauß, F.*, et al.* 2016. 3D reflection seismic imaging at the 2.5km deep COSC-1 scientific borehole, central Scandinavian

Caledonides. *Tectonophysics*, **689**, 40-55, http://doi.org/https://doi.org/10.1016/j.tecto.2015.12.013.

Heilman, E., Kolawole, F., Atekwana, E.A. & Mayle, M. 2019. Controls of Basement Fabric on the Linkage of Rift Segments. *Tectonics*, **0**, http://doi.org/10.1029/2018TC005362.

Henstra, G.A., Rotevatn, A., Gawthorpe, R.L. & Ravnås, R. 2015. Evolution of a major segmented normal fault during multiphase rifting: The origin of plan-view zigzag geometry. *Journal of Structural Geology*, **74**, 45-63, http://doi.org/https://doi.org/10.1016/j.jsg.2015.02.005.

Heron, P.J., Peace, A.L., McCaffrey, K., Welford, J.K., Wilson, R., van Hunen, J. & Pysklywec, R.N. 2019. Segmentation of rifts through structural inheritance: Creation of the Davis Strait. *Tectonics*, **0**, http://doi.org/10.1029/2019TC005578.

Higgs, K.E., Browne, G.H. & Sahoo, T.R. 2019. Reservoir characterisation of syn-rift and post-rift sandstones in frontier basins: An example from the Cretaceous of Canterbury and Great South basins, New Zealand. *Marine and Petroleum Geology*, **101**, 1-29, http://doi.org/https://doi.org/10.1016/j.marpetgeo.2018.11.030.

Howell, D.G. 1980. Mesozoic accretion of exotic terranes along the New Zealand segment of Gondwanaland. *Geology*, **8**, 487-491, http://doi.org/10.1130/0091-7613(1980)8<487:MAOETA>2.0.CO;2.

Howell, L., Egan, S., Leslie, G. & Clarke, S. 2019. Structural and geodynamic modelling of the influence of granite bodies during lithospheric extension: Application to the Carboniferous basins of northern England. *Tectonophysics*, http://doi.org/https://doi.org/10.1016/j.tecto.2019.02.008.

Jackson, C.A.L., Bell, R.E., Rotevatn, A. & Tvedt, A.B.M. 2017. Techniques to determine the kinematics of synsedimentary normal faults and implications for fault growth models. *Geological Society, London, Special Publications*, **439**, SP439.422, http://doi.org/10.1144/SP439.22.

Johnston, M.R. 2019. Chapter 2 The path to understanding the central terranes of Zealandia. *Geological Society, London, Memoirs*, **49**, 15-30, http://doi.org/10.1144/m49.2.

Jones, T.D. & Nur, A. 1984. The nature of seismic reflections from deep crustal fault zones. *Journal of Geophysical Research: Solid Earth*, **89**, 3153-3171, http://doi.org/10.1029/JB089iB05p03153.

Jongens, R. 2006. Structure of the Buller and Takaka Terrane rocks adjacent to the Anatoki Fault, northwest Nelson, New Zealand. *New Zealand Journal of Geology and Geophysics*, **49**, 443-461, http://doi.org/10.1080/00288306.2006.9515180.

Kim, Y.-S. & Sanderson, D.J. 2006. Structural similarity and variety at the tips in a wide range of strike–slip faults: a review. *Terra Nova*, **18**, 330-344, http://doi.org/10.1111/j.1365-3121.2006.00697.x.

Kirkpatrick, J.D., Bezerra, F.H.R., Shipton, Z.K., Do Nascimento, A.F., Pytharouli, S.I., Lunn, R.J. & Soden, A.M. 2013. Scale-dependent influence of pre-existing basement shear zones on rift faulting: a case study from NE Brazil. *Journal of the Geological Society*, **170**, 237, http://doi.org/10.1144/jgs2012-043.

Koopmann, H., Brune, S., Franke, D. & Breuer, S. 2014. Linking rift propagation barriers to excess magmatism at volcanic rifted margins. *Geology*, **42**, 1071-1074, http://doi.org/10.1130/G36085.1.

Kula, J., Tulloch, A., Spell, T.L. & Wells, M.L. 2007. Two-stage rifting of Zealandia-Australia-Antarctica: Evidence from 40Ar/39Ar thermochronometry of the Sisters shear zone, Stewart Island, New Zealand. *Geology*, **35**, 411-414, http://doi.org/10.1130/g23432a.1.

Kula, J., Tulloch, A.J., Spell, T.L., Wells, M.L. & Zanetti, K.A. 2009. Thermal evolution of the Sisters shear zone, southern New Zealand; Formation of the Great South Basin and onset of Pacific-Antarctic spreading. *Tectonics*, **28**, http://doi.org/10.1029/2008TC002368.

Landis, C.A., Campbell, H.J., Aslund, T., Cawood, P.A., Douglas, A., Kimbrough, D.L., Pillai, D.D.L., Raine, J.I., *et al.* 1999. Permian-Jurassic strata at Productus Creek, Southland, New Zealand: Implications for terrane dynamics of the eastern Gondwanaland margin. *New Zealand Journal of Geology and Geophysics*, **42**, 255-278, http://doi.org/10.1080/00288306.1999.9514844.

Lenhart, A., Jackson, C.A.L., Bell, R.E., Duffy, O.B., Gawthorpe, R.L. & Fossen, H. 2019. Structural architecture and composition of crystalline basement offshore west Norway. http://doi.org/10.1130/L668.1.

Long, J.J. & Imber, J. 2012. Strain compatibility and fault linkage in relay zones on normal faults. *Journal of Structural Geology*, **36**, 16-26, http://doi.org/https://doi.org/10.1016/j.jsg.2011.12.013.

Lundmark, A.M., Saether, T. & Sorlie, R. 2013. Ordovician to Silurian magmatism on the Utsira High, North Sea: implications for correlations between the onshore and offshore Caledonides. *Geological Society, London, Special Publications*, **390**, 513-523, http://doi.org/10.1144/sp390.21.

Lynn, H.B., Hale, L.D. & Thompson, G.A. 1981. Seismic Reflections from the Basal Contacts of Batholiths. *Journal of Geophysical Research*, **86**, 633-638, http://doi.org/10.1029/JB086iB11p10633.

Magee, C., McDermott, K.G., Stevenson, C.T.E. & Jackson, C.A.L. 2014. Influence of crystallised igneous intrusions on fault nucleation and reactivation during continental extension. *Journal of Structural Geology*, **62**, 183-193, http://doi.org/https://doi.org/10.1016/j.jsg.2014.02.003.

Mair, J.A. & Green, A.G. 1981. High-resolution seismic reflection profiles reveal fracture zones within a 'homogeneous' granite batholith. *Nature*, **294**, 439-442, http://doi.org/10.1038/294439a0.

McCaffrey, K.J.W. & Petford, N. 1997. Are granitic intrusions scale invariant? *Journal of the Geological Society*, **154**, 1, http://doi.org/10.1144/gsjgs.154.1.0001.

McLean, C.E., Schofield, N., Brown, D.J., Jolley, D.W. & Reid, A. 2017. 3D seismic imaging of the shallow plumbing system beneath the Ben Nevis Monogenetic Volcanic Field: Faroe–Shetland Basin. *Journal of the Geological Society*, **174**, 468, http://doi.org/10.1144/jgs2016-118.

McWilliams, M.O. & Howell, D.G. 1982. Exotic terranes of western California. *Nature*, **297**, 215-217, http://doi.org/10.1038/297215a0.

Morley, C.K. 2010. Stress re-orientation along zones of weak fabrics in rifts: An explanation for pure extension in 'oblique' rift segments? *Earth and Planetary Science Letters*, **297**, 667-673, http://doi.org/https://doi.org/10.1016/j.epsl.2010.07.022.

Morley, C.K. 2017. The impact of multiple extension events, stress rotation and inherited fabrics on normal fault geometries and evolution in the Cenozoic rift basins of Thailand. *Geological Society, London, Special Publications*, **439**, 413, http://doi.org/10.1144/SP439.3.

Morley, C.K., Haranya, C., Phoosongsee, W., Pongwapee, S., Kornsawan, A. & Wonganan, N. 2004. Activation of rift oblique and rift parallel pre-existing fabrics during extension and their effect on deformation style: examples from the rifts of Thailand. *Journal of Structural Geology*, **26**, 1803-1829, http://doi.org/https://doi.org/10.1016/j.jsg.2004.02.014.

Morley, C.K., Maczak, A., Rungprom, T., Ghosh, J., Cartwright, J.A., Bertoni, C. & Panpichityota, N. 2017. New style of honeycomb structures revealed on 3D seismic data indicate widespread diagenesis offshore Great South Basin, New Zealand. *Marine and Petroleum Geology*, **86**, 140-154, http://doi.org/10.1016/j.marpetgeo.2017.05.035.

Mortimer, E.J., Paton, D.A., Scholz, C.A. & Strecker, M.R. 2016. Implications of structural inheritance in oblique rift zones for basin compartmentalization: Nkhata Basin, Malawi Rift (EARS). *Marine and Petroleum Geology*, **72**, 110-121, http://doi.org/https://doi.org/10.1016/j.marpetgeo.2015.12.018.

Mortimer, N. 2004. New Zealand's Geological Foundations. *Gondwana Research*, **7**, 261-272, http://doi.org/https://doi.org/10.1016/S1342-937X(05)70324-5.

Mortimer, N. 2014. The oroclinal bend in the South Island, New Zealand. *Journal of Structural Geology*, **64**, 32-38, http://doi.org/https://doi.org/10.1016/j.jsg.2013.08.011.

Mortimer, N., Tulloch, A.J. & Ireland, T.R. 1997. Basement geology of Taranaki and Wanganui Basins, New Zealand. *New Zealand Journal of Geology and Geophysics*, **40**, 223-236, http://doi.org/10.1080/00288306.1997.9514754.

Mortimer, N., Davey, F.J., Melhuish, A., Yu, J. & Godfrey, N.J. 2002. Geological interpretation of a deep seismic reflection profile across the Eastern Province and Median Batholith, New Zealand: Crustal architecture of an extended Phanerozoic convergent orogen. *New Zealand Journal of Geology and Geophysics*, **45**, 349-363, http://doi.org/10.1080/00288306.2002.9514978.

Mortimer, N., Tulloch, A.J., Spark, R.N., Walker, N.W., Ladley, E., Allibone, A. & Kimbrough, D.L. 1999. Overview of the Median Batholith, New Zealand: a new interpretation of the geology of the Median Tectonic Zone and adjacent rocks. *Journal of African Earth Sciences*, **29**, 257-268, http://doi.org/https://doi.org/10.1016/S0899-5362(99)00095-0.

Mouslopoulou, V., Nicol, A., Little, T.A. & Walsh, J.J. 2007. Displacement transfer between intersecting regional strike-slip and extensional fault systems. *Journal of Structural Geology*, **29**, 100-116, http://doi.org/https://doi.org/10.1016/j.jsg.2006.08.002.

Muir, R.J., Bradshaw, J.D., Weaver, S.D. & Laird, M.G. 2000. The influence of basement structure on the evolution of the Taranaki Basin, New Zealand. *Journal of the Geological Society*, **157**, 1179, http://doi.org/10.1144/jgs.157.6.1179.

Nicol, A., Childs, C., Walsh, J.J., Manzocchi, T. & Schöpfer, M.P.J. 2017. Interactions and growth of faults in an outcrop-scale system. *Geological Society, London, Special Publications*, **439**, 23, http://doi.org/10.1144/SP439.9.

Nixon, C.W., Bull, J.M. & Sanderson, D.J. 2014. Localized vs distributed deformation associated with the linkage history of an active normal fault, Whakatane Graben, New Zealand. *Journal of Structural Geology*, **69**, 266-280, http://doi.org/https://doi.org/10.1016/j.jsg.2014.06.005.

Norris, R.J. & Cooper, A.F. 2001. Late Quaternary slip rates and slip partitioning on the Alpine Fault, New Zealand. *Journal of Structural Geology*, **23**, 507-520, http://doi.org/https://doi.org/10.1016/S0191-8141(00)00122-X.

Paton, D.A. & Underhill, J.R. 2004. Role of crustal anisotropy in modifying the structural and sedimentological evolution of extensional basins: the Gamtoos Basin, South Africa. *Basin Research*, **16**, 339-359, http://doi.org/10.1111/j.1365-2117.2004.00237.x.

Paton, D.A., Mortimer, E.J., Hodgson, N. & van der Spuy, D. 2016. The missing piece of the South Atlantic jigsaw: when continental break-up ignores crustal heterogeneity. *Geological Society, London, Special Publications*, **438**, SP438.438, http://doi.org/10.1144/SP438.8.

Peace, A., McCaffrey, K., Imber, J., van Hunen, J., Hobbs, R. & Wilson, R. 2017. The role of pre-existing structures during rifting, continental breakup and transform system development, offshore West Greenland. *Basin Research*, 373-394, http://doi.org/ https://doi.org/10.1111/bre.12257.

Perrin, C., Manighetti, I. & Gaudemer, Y. 2016. Off-fault tip splay networks: A genetic and generic property of faults indicative of their long-term propagation. *Comptes Rendus Geoscience*, **348**, 52-60, http://doi.org/https://doi.org/10.1016/j.crte.2015.05.002.

Petford, N. & Atherton, M.P. 1992. Granitoid emplacement and deformation along a major crustal lineament: The Cordillera Blanca, Peru. *Tectonophysics*, **205**, 171-185, http://doi.org/https://doi.org/10.1016/0040-1951(92)90425-6.

Petford, N., Cruden, A.R., McCaffrey, K.J.W. & Vigneresse, J.L. 2000. Granite magma formation, transport and emplacement in the Earth's crust. *Nature*, **408**, 669-673, http://doi.org/10.1038/35047000.

Philippon, M., Willingshofer, E., Sokoutis, D., Corti, G., Sani, F., Bonini, M. & Cloetingh, S. 2015. Slip re-orientation in oblique rifts. *Geology*, **43**, 147-150, http://doi.org/10.1130/G36208.1.

Phillips, T.B., Magee, C., Jackson, C.A.L. & Bell, R.E. 2017. Determining the three-dimensional geometry of a dike swarm and its impact on later rift geometry using seismic reflection data. *Geology*, **46**, 119-122, http://doi.org/10.1130/G39672.1.

Phillips, T.B., Jackson, C.A.L., Bell, R.E. & Duffy, O.B. 2018. Oblique reactivation of lithosphere-scale lineaments controls rift physiography – the upper-crustal expression of the Sorgenfrei–Tornquist Zone, offshore southern Norway. *Solid Earth*, **9**, 403-429, http://doi.org/10.5194/se-9-403-2018.

Phillips, T.B., Jackson, C.A., Bell, R.E., Duffy, O.B. & Fossen, H. 2016. Reactivation of intrabasement structures during rifting: A case study from offshore southern Norway. *Journal of Structural Geology*, **91**, 54-73, http://doi.org/10.1016/j.jsg.2016.08.008.

Reeve, M.T., Bell, R.E. & Jackson, C.A.L. 2013. Origin and significance of intra-basement seismic reflections offshore western Norway. *Journal of the Geological Society*, **171**, 1-4, http://doi.org/10.1144/jgs2013-020.

Rennie, S.F., Fagereng, Å. & Diener, J.F.A. 2013. Strain distribution within a km-scale, mid-crustal shear zone: The Kuckaus Mylonite Zone, Namibia. *Journal of Structural Geology*, **56**, 57-69, http://doi.org/https://doi.org/10.1016/j.jsg.2013.09.001.

Ring, U.W.E., Schwartz, H.L., Bromage, T.G. & Sanaane, C. 2005. Kinematic and sedimentological evolution of the Manyara Rift in northern Tanzania, East Africa. *Geological Magazine*, **142**, 355-368, http://doi.org/10.1017/S0016756805000841.

Robertson, A.H.F. & Palamakumbura, R. 2019. Chapter 9 Sedimentary development of the Mid-Permian–Mid-Triassic Maitai continental margin forearc basin, South Island, New Zealand. *Geological Society, London, Memoirs*, **49**, 189-230, http://doi.org/10.1144/m49.9.

Robertson, A.H.F., Campbell, H.J., Johnston, M.R. & Palamakumbra, R. 2019. Chapter 15 Construction of a Paleozoic–Mesozoic accretionary orogen along the active continental margin of SE Gondwana (South Island, New Zealand): summary and overview. *Geological Society, London, Memoirs*, **49**, 331-372, http://doi.org/10.1144/m49.8.

Rotevatn, A., Jackson, C.A.L., Tvedt, A.B.M., Bell, R.E. & Blækkan, I. 2018a. How do normal faults grow? *Journal of Structural Geology*, http://doi.org/https://doi.org/10.1016/j.jsg.2018.08.005.

Rotevatn, A., Kristensen, T.B., Ksienzyk, A.K., Wemmer, K., Henstra, G.A., Midtkandal, I., Grundvåg, S.-A. & Andresen, A. 2018b. Structural Inheritance and Rapid Rift-Length Establishment in a

Multiphase Rift: The East Greenland Rift System and its Caledonian Orogenic Ancestry. *Tectonics*, **37**, 1858-1875, http://doi.org/doi:10.1029/2018TC005018.

Sahoo, T., King, P., Bland, K., Strogen, D., Sykes, R. & Bache, F. 2014. Tectono-sedimentary evolution and source rock distribution of the mid to Late Cretaceous succession in the Great South Basin, New Zealand *The APPEA Journal*, **54**, 259-274, http://doi.org/https://doi.org/10.1071/AJ13026.

Samsu, A., Cruden, A.R., Hall, M., Micklethwaite, S. & Denyszyn, S.W. 2019. The influence of basement faults on local extension directions: Insights from potential field geophysics and field observations. *Basin Research*, **0**, http://doi.org/10.1111/bre.12344.

Schwartz, J.J., Johnson, K., Mueller, P., Strickland, A., Valley, J. & Wooden, J.L. 2014. Time scales and processes of Cordilleran batholith construction and high-Sr/Y magmatic pulses: Evidence from the Bald Mountain batholith, northeastern Oregon. *Geosphere*, **10**, 1456-1481, http://doi.org/10.1130/GES01033.1.

Slagstad, T., Davidsen, B. & Daly, J.S. 2011. Age and composition of crystalline basement rocks on the Norwegian continental margin: offshore extension and continuity of the Caledonian–Appalachian orogenic belt. *Journal of the Geological Society*, **168**, 1167, http://doi.org/10.1144/0016-76492010-136.

Sutherland, R., Davey, F. & Beavan, J. 2000. Plate boundary deformation in South Island, New Zealand, is related to inherited lithospheric structure. *Earth and Planetary Science Letters*, **177**, 141-151, http://doi.org/https://doi.org/10.1016/S0012-821X(00)00043-1.

Sutherland, R., Collot, J., Lafoy, Y., Logan, G.A., Hackney, R., Stagpoole, V., Uruski, C., Hashimoto, T., *et al.* 2010. Lithosphere delamination with foundering of lower crust and mantle caused permanent subsidence of New Caledonia Trough and transient uplift of Lord Howe Rise during Eocene and Oligocene initiation of Tonga-Kermadec subduction, western Pacific. *Tectonics*, **29**, http://doi.org/10.1029/2009TC002476.

Thomas, W.A. 2006. Tectonic inheritance at a continental margin. *GSA Today*, **16**, 4-11, http://doi.org/10.1130/1052-5173(2006)016<4:TIAACM>2.0.CO;2.

Thomas, W.A. 2018. Tectonic inheritance at multiple scales during more than two complete Wilson cycles recorded in eastern North America. *Geological Society, London, Special Publications*, **470**, SP470.474, http://doi.org/10.1144/SP470.4.

Tommasi, A. & Vauchez, A. 2001. Continental rifting parallel to ancient collisional belts: an effect of the mechanical anisotropy of the lithospheric mantle. *Earth and Planetary Science Letters*, **185**, 199-210, http://doi.org/10.1016/S0012-821x(00)00350-2.

Tulloch, A., Mortimer, N., Ireland, T., Waight, T., Maas, R., Palin, M., Sahoo, T., Seebeck, H., *et al.* 2019. Reconnaissance basement geology and tectonics of South Zealandia. *Tectonics*, **0**, http://doi.org/10.1029/2018TC005116.

Tulloch, A.J. 1988. Batholiths, plutons, and suites: nomenclature for granitoid rocks of Westland—Nelson, New Zealand. *New Zealand Journal of Geology and Geophysics*, **31**, 505-509, http://doi.org/10.1080/00288306.1988.10422147.

Tulloch, A.J., Kimbrough, D.L., Landis, C.A., Mortimer, N. & Johnston, M.R. 1999. Relationships between the brook street Terrane and Median Tectonic Zone (Median Batholith): Evidence from Jurassic conglomerates. *New Zealand Journal of Geology and Geophysics*, **42**, 279-293, http://doi.org/10.1080/00288306.1999.9514845.

Tulloch, A.J., Ramezani, J., Kimbrough, D.L., Faure, K. & Allibone, A.H. 2009. U-Pb geochronology of mid-Paleozoic plutonism in western New Zealand: Implications for S-type granite generation and growth of the east Gondwana marginU-Pb geochronology of Paleozoic plutonism, New Zealand. *GSA Bulletin*, **121**, 1236-1261, http://doi.org/10.1130/B26272.1.

Uruski, C. 2015. The contribution of offshore seismic data to understanding the evolution of the New Zealand continent. *Sedimentary Basins and Crustal Processes at Continental Margins: From Modern Hyper-Extended Margins to Deformed Ancient Analogues*, **413**, 35-51, http://doi.org/10.1144/Sp413.1.

Uruski, C., Kennedy, C., Harrison, T., Maslen, G., Cook, R., Sutherland, R. & Zhu, H. 2007. Petroleum potential of the Great South Basin, New Zealand—New seismic data improves imaging. *The APPEA Journal*, **47**, 145-161, http://doi.org/https://doi.org/10.1071/AJ06008.

Uruski, C.I. 2010. New Zealand's deepwater frontier. *Marine and Petroleum Geology*, **27**, 2005-2026, http://doi.org/https://doi.org/10.1016/j.marpetgeo.2010.05.010.

Van Buer, N.J., Miller, E.L. & Dumitru, T.A. 2009. Early Tertiary paleogeologic map of the northern Sierra Nevada batholith and the northwestern Basin and Range. *Geology*, **37**, 371-374, http://doi.org/10.1130/g25448a.1.

Vasconcelos, D.L., Bezerra, F.H.R., Medeiros, W.E., de Castro, D.L., Clausen, O.R., Vital, H. & Oliveira, R.G. 2019. Basement fabric controls rift nucleation and postrift basin inversion in the continental margin of NE Brazil. *Tectonophysics*, **751**, 23-40, http://doi.org/https://doi.org/10.1016/j.tecto.2018.12.019.

Walsh, J.J. & Watterson, J. 1991. Geometric and kinematic coherence and scale effects in normal fault systems. *Geological Society, London, Special Publications*, **56**, 193-203, http://doi.org/https://doi.org/10.1144/GSL.SP.1991.056.01.13.

Walsh, J.J., Nicol, A. & Childs, C. 2002. An alternative model for the growth of faults. *Journal of Structural Geology*, **24**, 1669-1675, http://doi.org/https://doi.org/10.1016/S0191-8141(01)00165-1.

Walsh, J.J., Watterson, J., Childs, C. & Nicol, A. 1996. Ductile strain effects in the analysis of seismic interpretations of normal fault systems. *Geological Society, London, Special Publications*, **99**, 27, http://doi.org/10.1144/GSL.SP.1996.099.01.04.

Walsh, J.J., Bailey, W.R., Childs, C., Nicol, A. & Bonson, C.G. 2003. Formation of segmented normal faults: a 3-D perspective. *Journal of Structural Geology*, **25**, 1251-1262, http://doi.org/https://doi.org/10.1016/S0191-8141(02)00161-X.

Wang, C.-Y., Okaya, D.A., Ruppert, C., Davis, G.A., Guo, T.-S., Zhong, Z. & Wenk, H.-R. 1989. Seismic reflectivity of the Whipple Mountain shear zone in southern California. *Journal of Geophysical Research: Solid Earth*, **94**, 2989-3005, http://doi.org/10.1029/JB094iB03p02989.

Wannamaker, P.E., Caldwell, T.G., Jiracek, G.R., Maris, V., Hill, G.J., Ogawa, Y., Bibby, H.M., Bennie, S.L.*, et al.* 2009. Fluid and deformation regime of an advancing subduction system at Marlborough, New Zealand. *Nature*, **460**, 733, http://doi.org/10.1038/nature08204

https://www.nature.com/articles/nature08204#supplementary-information.

Wellman, H.W. 1953. Data for the study of recent and late Pleistocene faulting in the South Island of New Zealand. *New Zealand Journal of Science and Technology*, **34 B**, 270-288.

Wenker, S. & Beaumont, C. 2016. Effects of lateral strength contrasts and inherited heterogeneities on necking and rifting of continents. *Tectonophysics*, http://doi.org/https://doi.org/10.1016/j.tecto.2016.10.011.

Whipp, P.S., Jackson, C.A.L., Gawthorpe, R.L., Dreyer, T. & Quinn, D. 2014. Normal fault array evolution above a reactivated rift fabric; a subsurface example from the northern Horda Platform, Norwegian North Sea. *Basin Research*, **26**, 523-549, http://doi.org/10.1111/bre.12050.

Wilson, J.T. 1966. Did the Atlantic Close and then Re-Open? *Nature*, **211**, 676-681, http://doi.org/10.1038/211676a0.

Figures

Figure 1

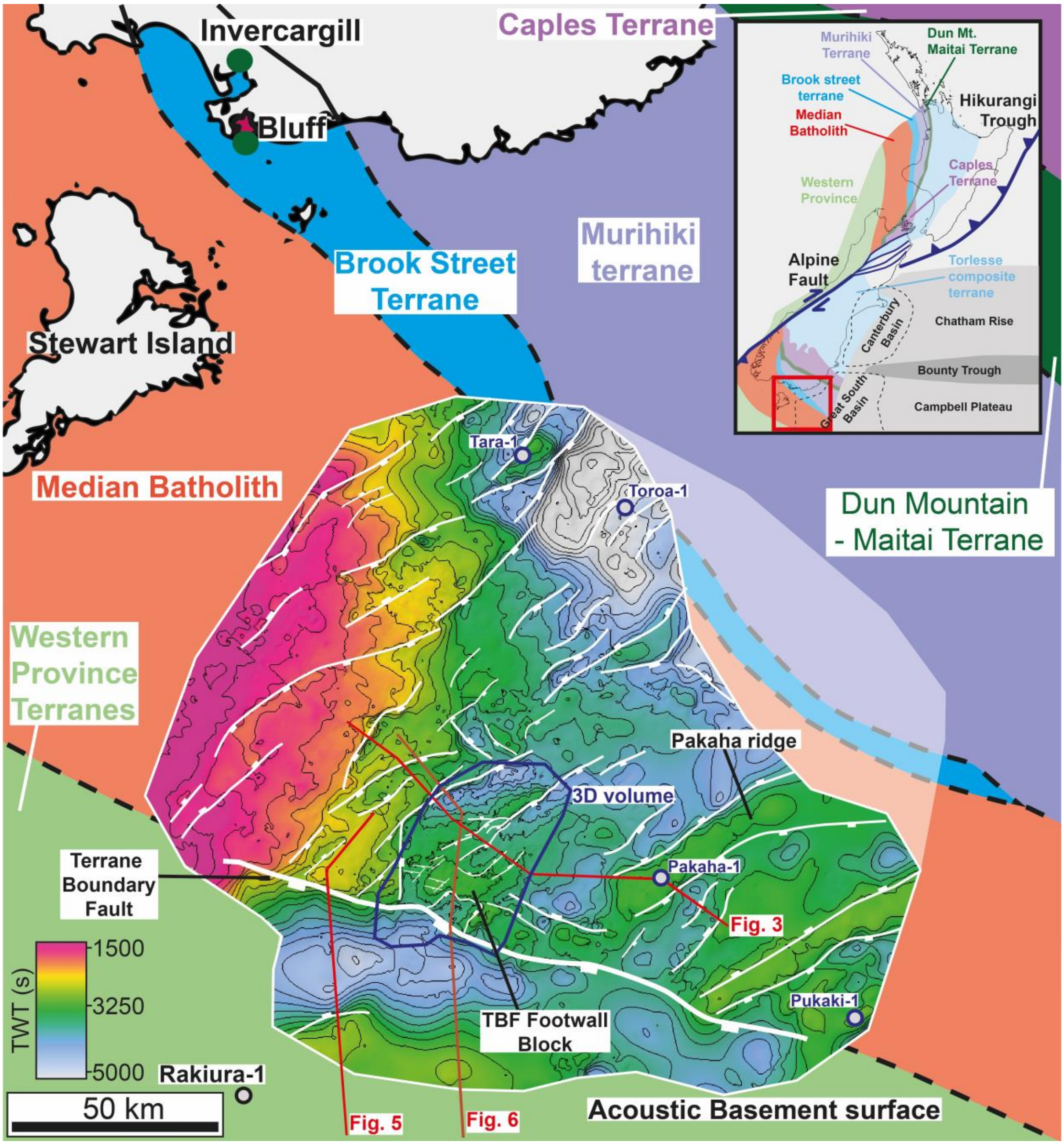

Invercargill
Bluff
Caples Terrane
Murihiki terrane
Brook Street Terrane
Stewart Island
Median Batholith
Dun Mountain - Maitai Terrane
Western Province Terranes
Tara-1
Toroa-1
Pakaha ridge
3D volume
Pakaha-1
Fig. 3
Terrane Boundary Fault
TWT (s)
1500
3250
5000
Rakiura-1
50 km
TBF Footwall Block
Pukaki-1
Fig. 5
Fig. 6
Acoustic Basement surface
Murihiki Terrane
Dun Mt. Maitai Terrane
Brook street terrane
Median Batholith
Hikurangi Trough
Caples Terrane
Western Province
Alpine Fault
Torlesse composite terrane
Chatham Rise
Canterbury Basin
Bounty Trough
Great South Basin
Campbell Plateau

1306 Figure 2

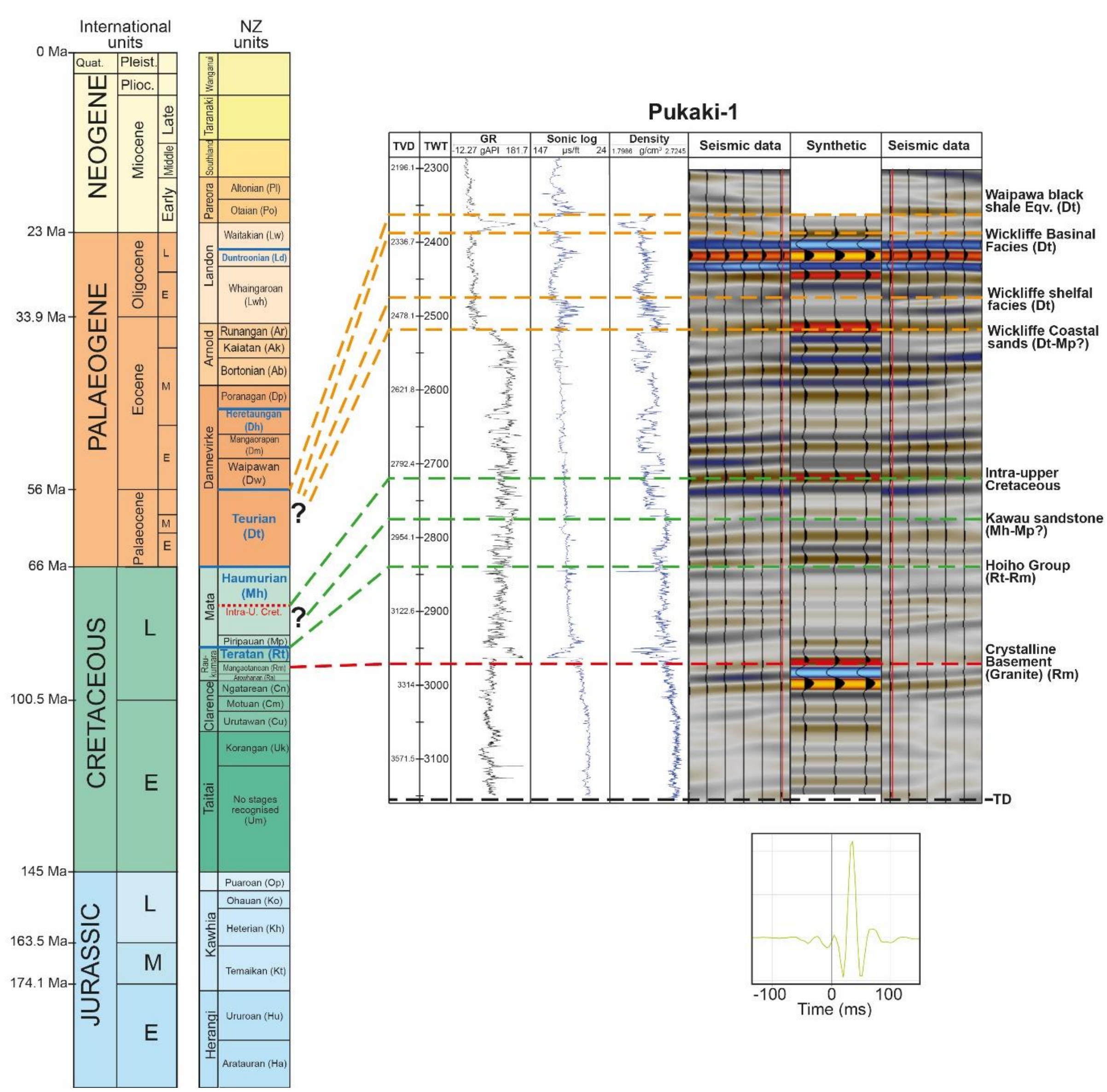

1307

1308

1309

Figure 3

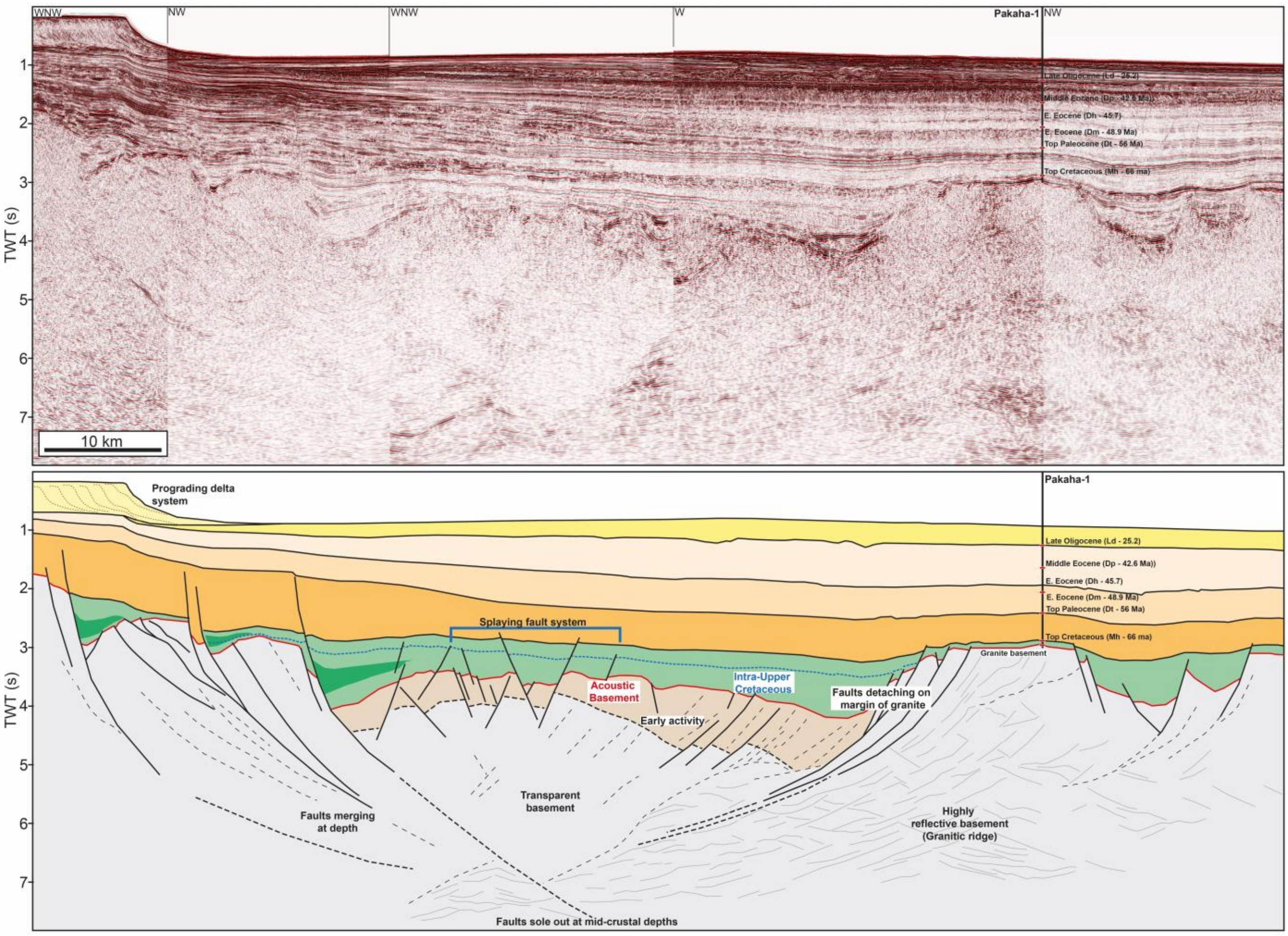

WNW
NW
WNW
W
Pakaha-1
NW
TWT (s)
10 km
Prograding delta system
Pakaha-1
Late Oligocene (Ld - 25.2)
Middle Eocene (Dp - 42.6 Ma))
E. Eocene (Dh - 45.7)
E. Eocene (Dm - 48.9 Ma)
Top Paleocene (Dt - 56 Ma)
Top Cretaceous (Mh - 66 ma)
Granite basement
Splaying fault system
Acoustic Basement
Intra-Upper Cretaceous
Faults detaching on margin of granite
Early activity
Transparent basement
Faults merging at depth
Highly reflective basement (Granitic ridge)
Faults sole out at mid-crustal depths

Figure 4

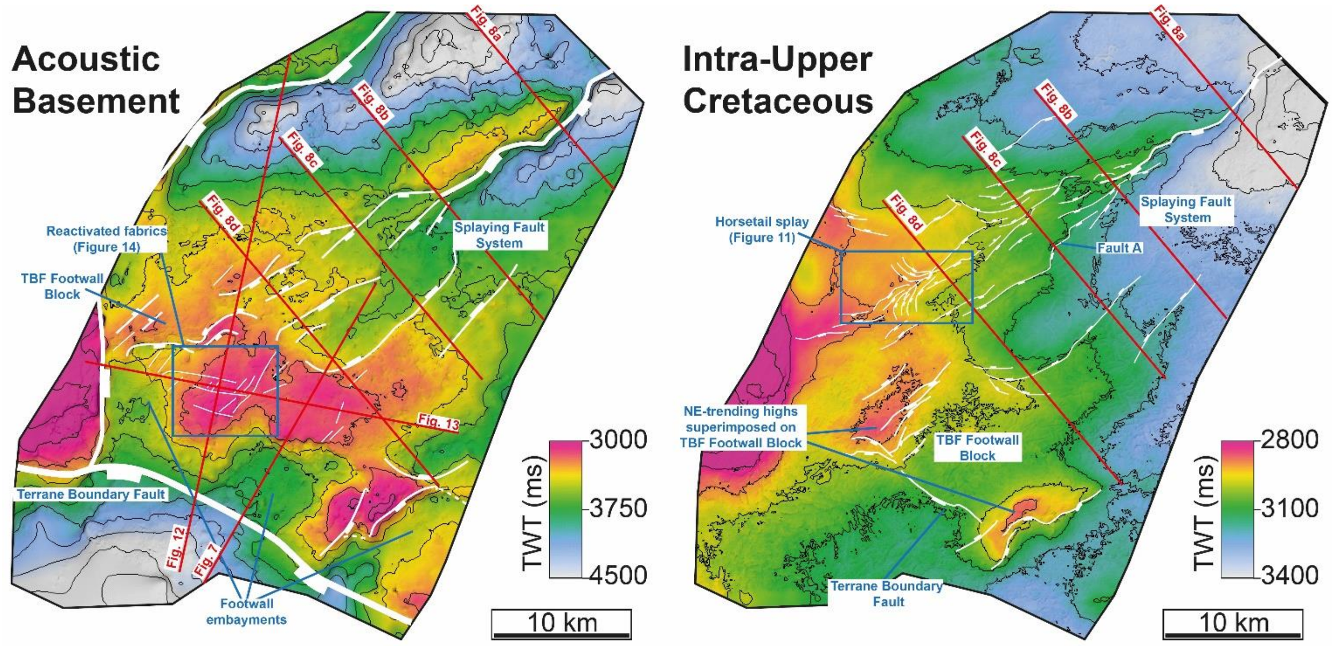
Acoustic Basement
Fig. 8a
Fig. 8b
Fig. 8c
Fig. 8d
Fig. 13
Fig. 12
Fig. 7
Reactivated fabrics (Figure 14)
TBF Footwall Block
Splaying Fault System
Terrane Boundary Fault
Footwall embayments
TWT (ms)
3000
3750
4500
10 km
Intra-Upper Cretaceous
Horsetail splay (Figure 11)
Splaying Fault System
Fault A
NE-trending highs superimposed on TBF Footwall Block
TBF Footwall Block
Terrane Boundary Fault
TWT (ms)
2800
3100
3400
10 km

Figure 5

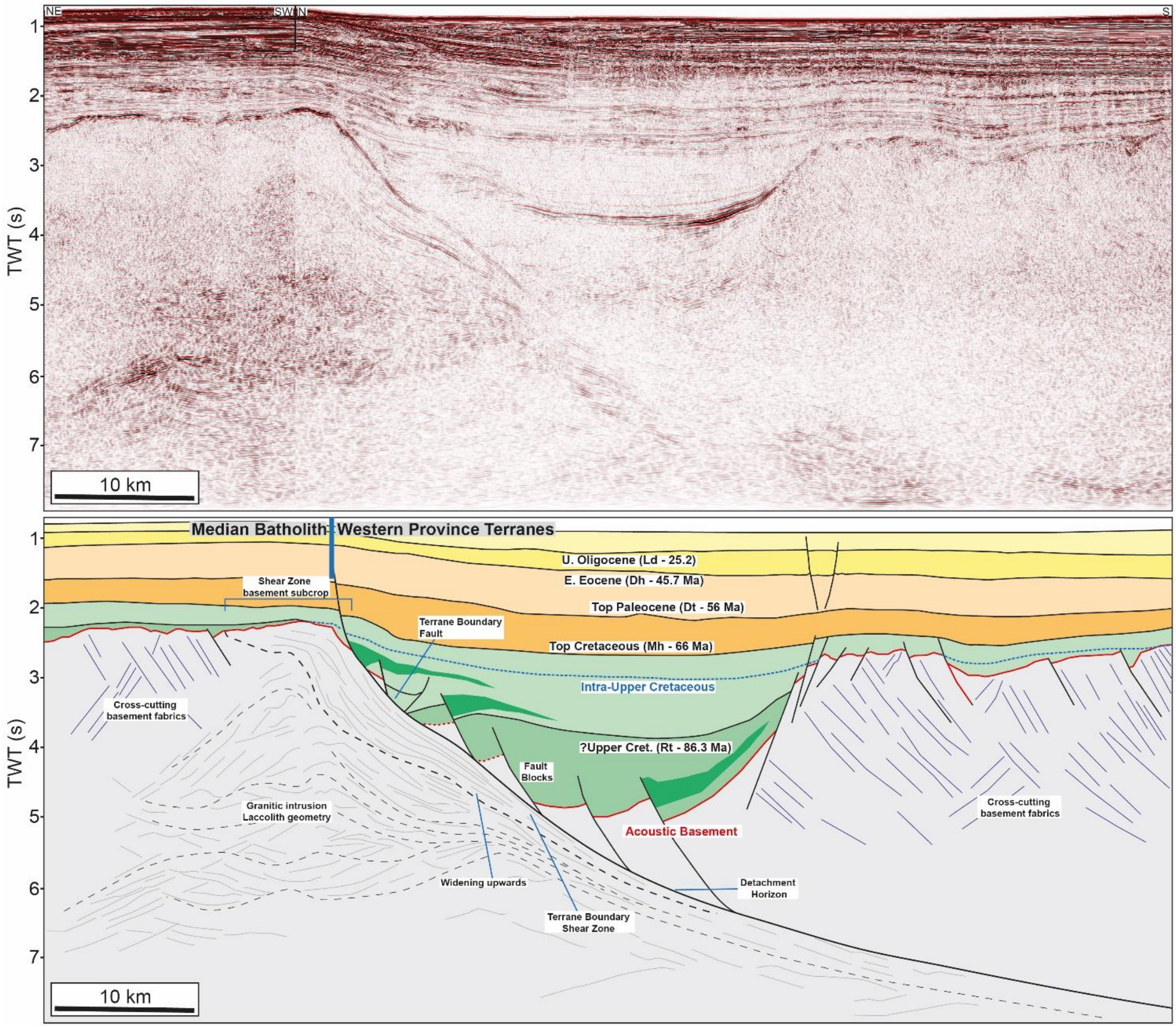
NE
SW
N
S
TWT (s)
10 km
Median Batholith
Western Province Terranes
U. Oligocene (Ld - 25.2)
E. Eocene (Dh - 45.7 Ma)
Top Paleocene (Dt - 56 Ma)
Top Cretaceous (Mh - 66 Ma)
Intra-Upper Cretaceous
?Upper Cret. (Rt - 86.3 Ma)
Acoustic Basement
Shear Zone basement subcrop
Terrane Boundary Fault
Cross-cutting basement fabrics
Fault Blocks
Granitic intrusion Laccolith geometry
Widening upwards
Terrane Boundary Shear Zone
Detachment Horizon
Cross-cutting basement fabrics

Figure 6

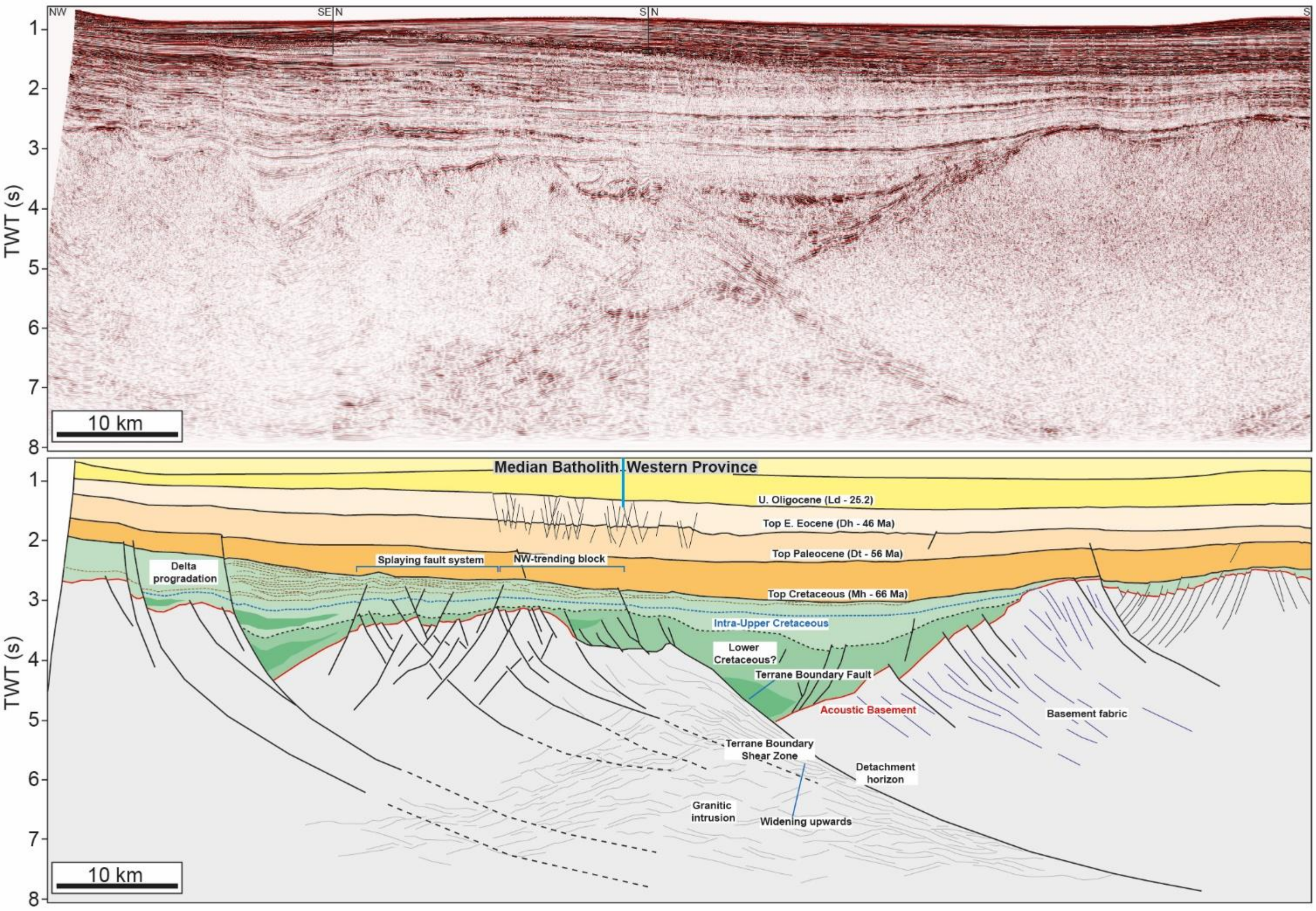
NW
SE
N
S
N
S
TWT (s)
10 km
Median Batholith
Western Province
U. Oligocene (Ld - 25.2)
Top E. Eocene (Dh - 46 Ma)
Top Paleocene (Dt - 56 Ma)
Top Cretaceous (Mh - 66 Ma)
Intra-Upper Cretaceous
Delta progradation
Splaying fault system
NW-trending block
Lower Cretaceous?
Terrane Boundary Fault
Acoustic Basement
Basement fabric
Terrane Boundary Shear Zone
Detachment horizon
Granitic intrusion
Widening upwards

1322 Figure 7

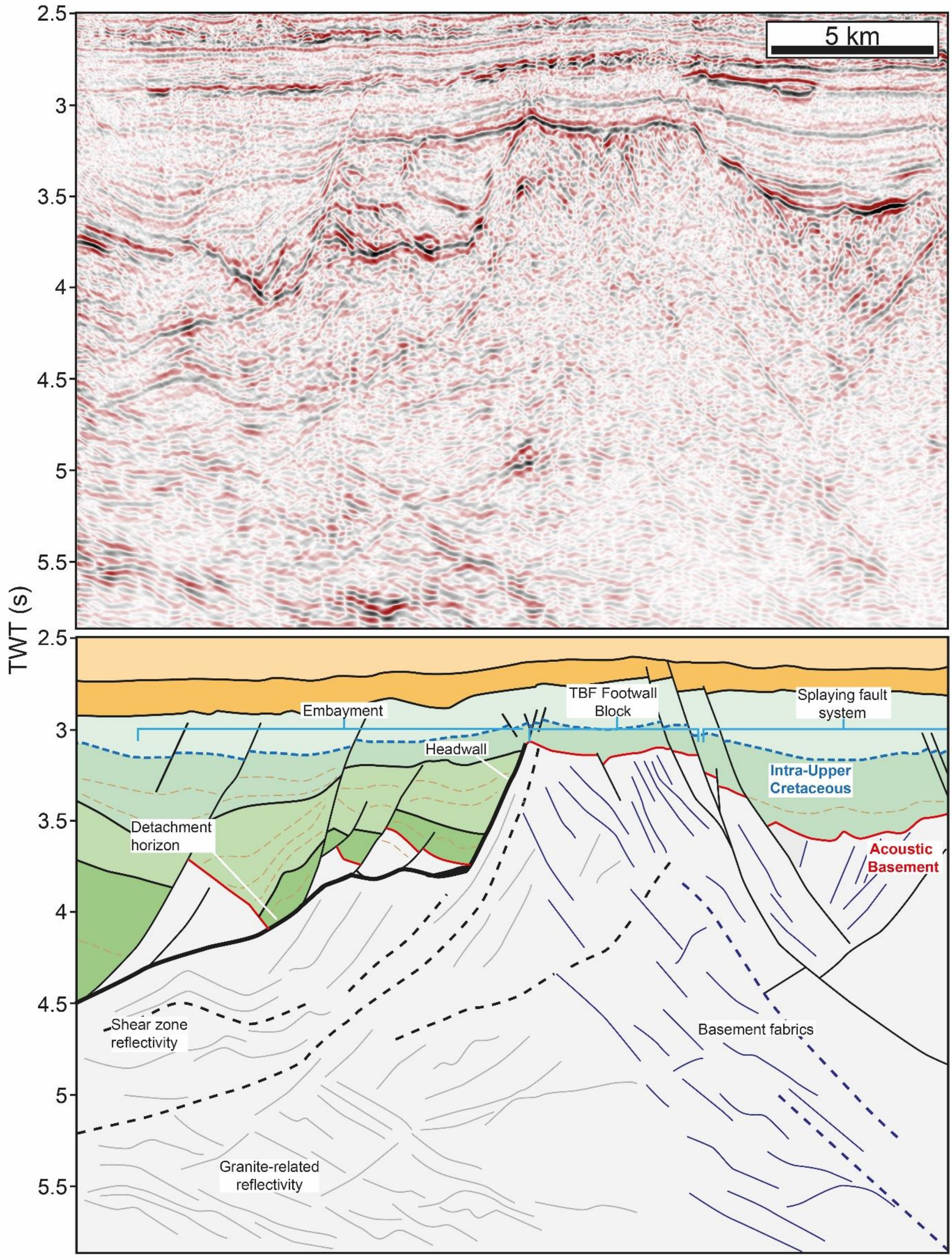

1323

1324

Figure 8

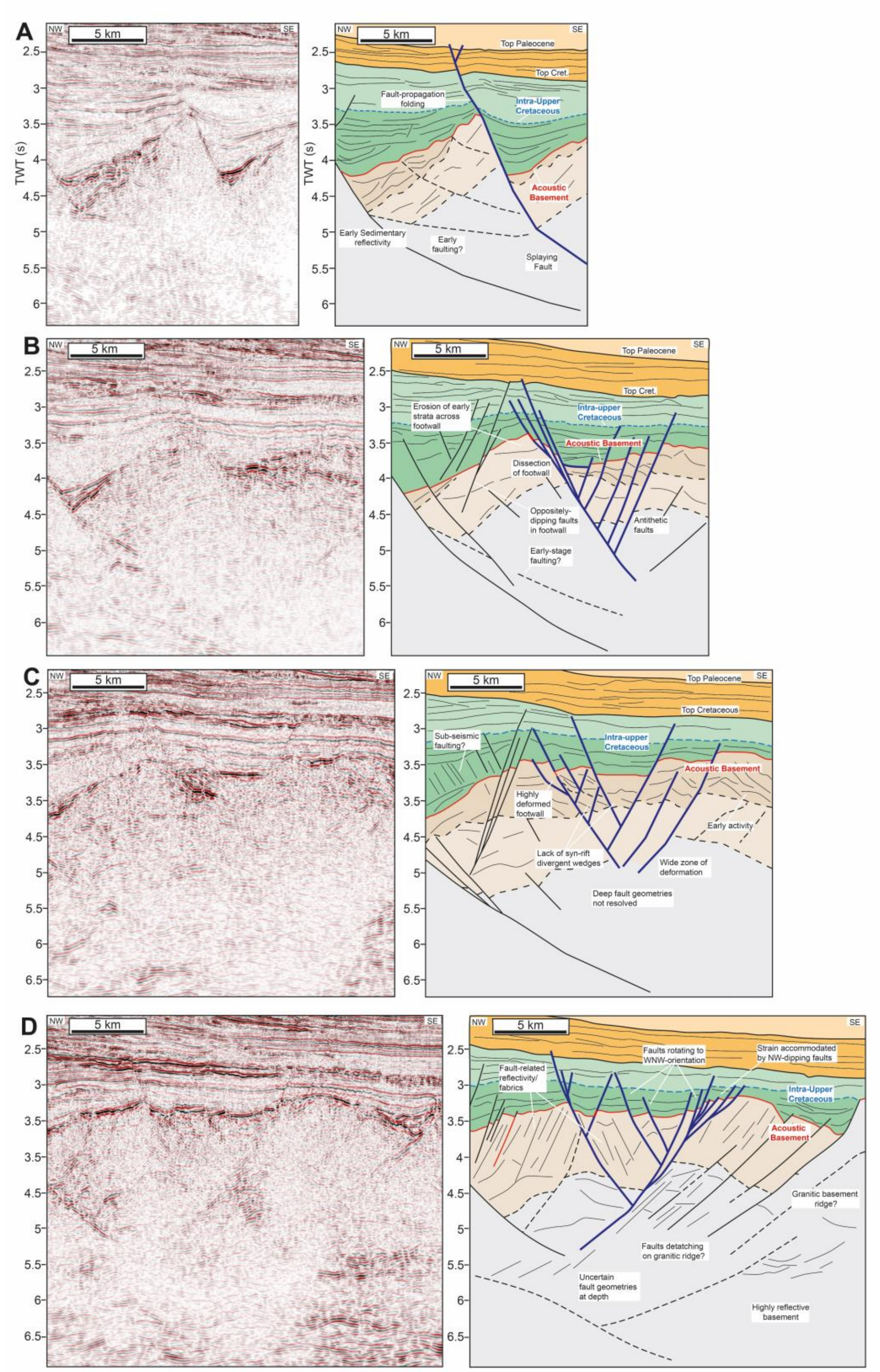

A
B
C
D
NW
SE
5 km
TWT (s)
Top Paleocene
Top Cret.
Top Cretaceous
Fault-propagation folding
Intra-Upper Cretaceous
Intra-upper Cretaceous
Acoustic Basement
Early Sedimentary reflectivity
Early faulting?
Splaying Fault
Erosion of early strata across footwall
Dissection of footwall
Oppositely-dipping faults in footwall
Antithetic faults
Early-stage faulting?
Sub-seismic faulting?
Highly deformed footwall
Lack of syn-rift divergent wedges
Wide zone of deformation
Early activity
Deep fault geometries not resolved
Fault-related reflectivity/ fabrics
Faults rotating to WNW-orientation
Strain accommodated by NW-dipping faults
Granitic basement ridge?
Faults detatching on granitic ridge?
Uncertain fault geometries at depth
Highly reflective basement

Figure 9

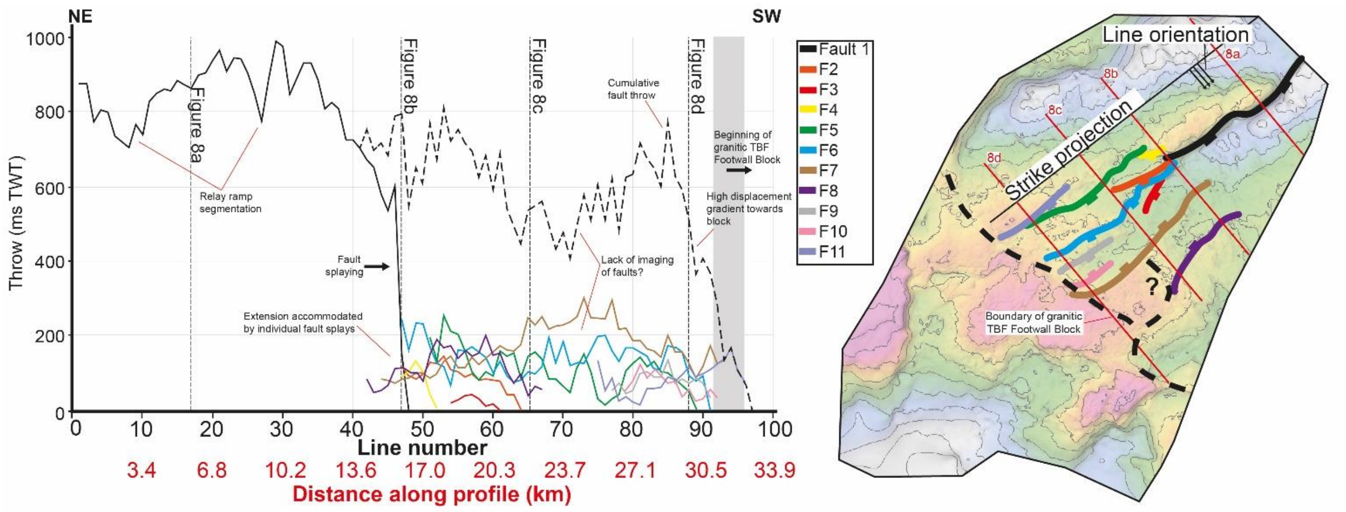

NE
SW
Throw (ms TWT)
1000
800
600
400
200
0
Figure 8a
Figure 8b
Figure 8c
Figure 8d
Relay ramp segmentation
Fault splaying
Extension accommodated by individual fault splays
Cumulative fault throw
Lack of imaging of faults?
Beginning of granitic TBF Footwall Block
High displacement gradient towards block
0
10
20
30
40
50
60
70
80
90
100
Line number
3.4
6.8
10.2
13.6
17.0
20.3
23.7
27.1
30.5
33.9
Distance along profile (km)
Fault 1
F2
F3
F4
F5
F6
F7
F8
F9
F10
F11
Line orientation
Strike projection
8a
8b
8c
8d
?
Boundary of granitic TBF Footwall Block

Figure 10

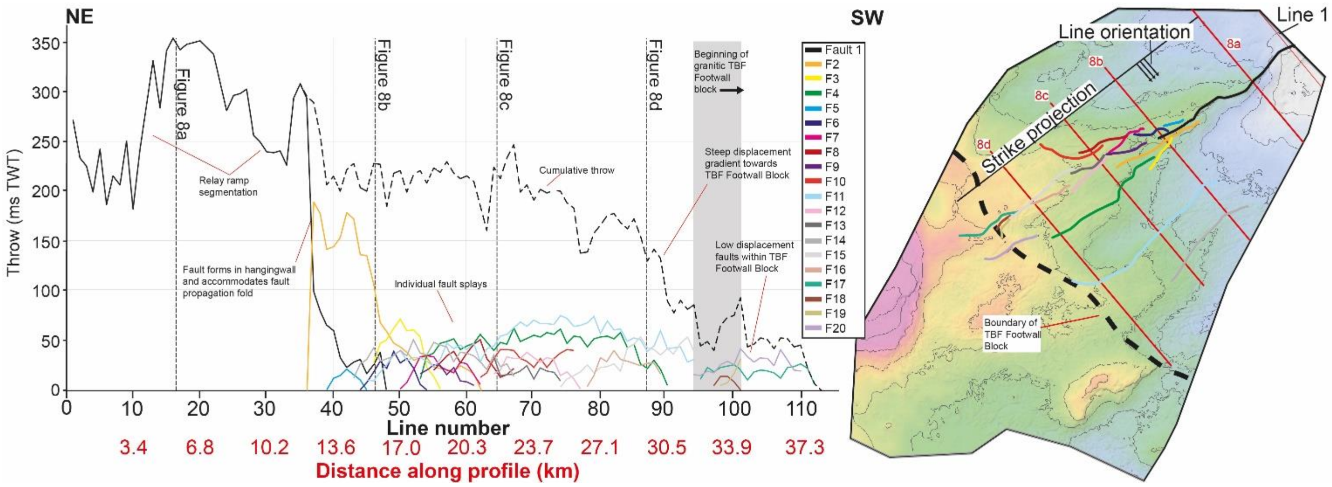
NE
SW
Throw (ms TWT)
350
300
250
200
150
100
50
0
Figure 8a
Figure 8b
Figure 8c
Figure 8d
Beginning of granitic TBF Footwall block
Relay ramp segmentation
Cumulative throw
Steep displacement gradient towards TBF Footwall Block
Low displacement faults within TBF Footwall Block
Fault forms in hangingwall and accommodates fault propagation fold
Individual fault splays
Fault 1
F2
F3
F4
F5
F6
F7
F8
F9
F10
F11
F12
F13
F14
F15
F16
F17
F18
F19
F20
0
10
20
30
40
50
60
70
80
90
100
110
Line number
3.4
6.8
10.2
13.6
17.0
20.3
23.7
27.1
30.5
33.9
37.3
Distance along profile (km)
Line 1
Line orientation
8a
8b
8c
8d
Strike projection
Boundary of TBF Footwall Block

Figure 11

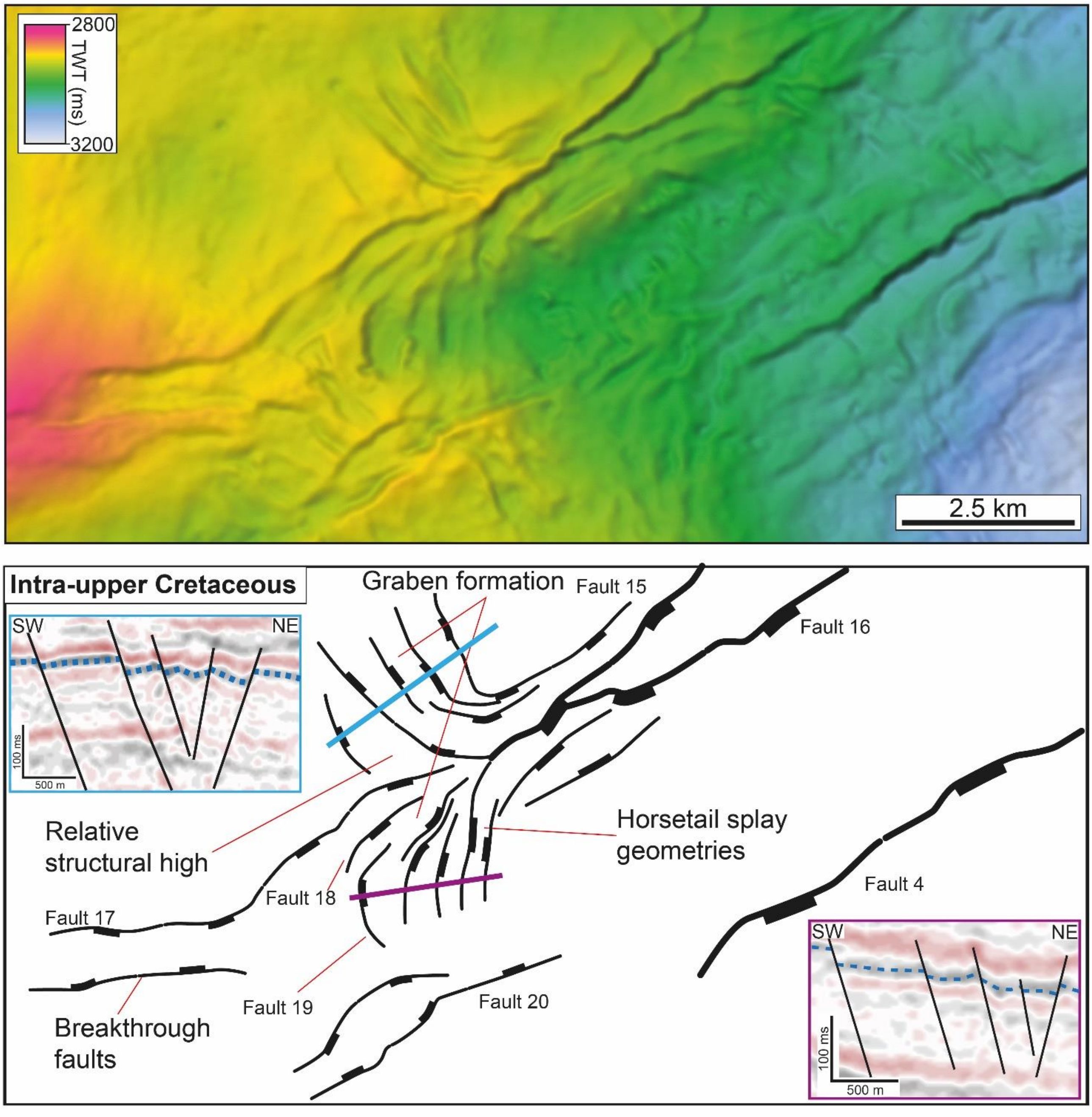
2800
TWT (ms)
3200
2.5 km
Intra-upper Cretaceous
Graben formation
Fault 15
Fault 16
SW
NE
100 ms
500 m
Relative structural high
Horsetail splay geometries
Fault 4
Fault 17
Fault 18
Fault 19
Fault 20
Breakthrough faults

Figure 12

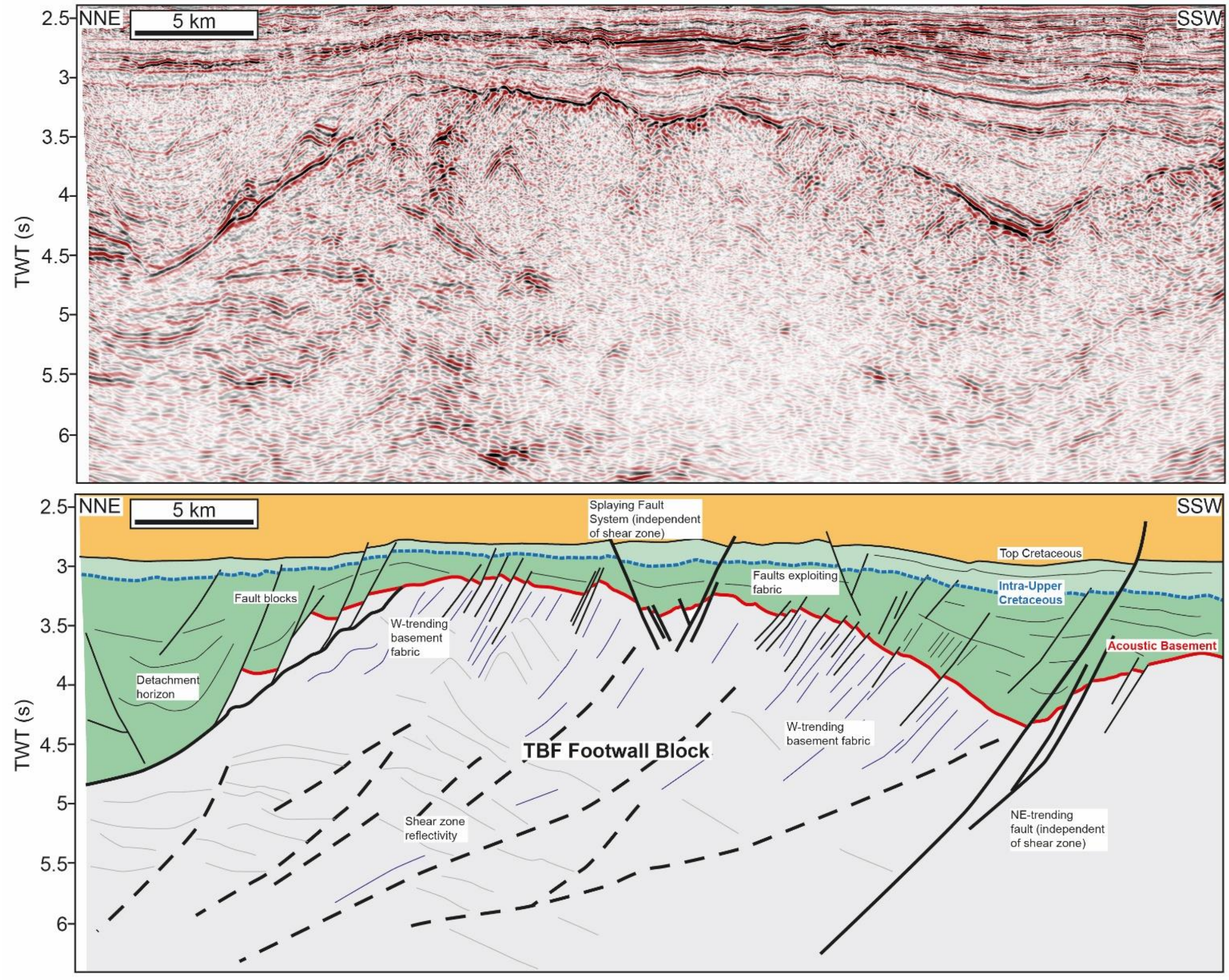

NNE
5 km
SSW
TWT (s)
2.5
3
3.5
4
4.5
5
5.5
6
Splaying Fault System (independent of shear zone)
Top Cretaceous
Intra-Upper Cretaceous
Acoustic Basement
Fault blocks
Faults exploiting fabric
W-trending basement fabric
Detachment horizon
TBF Footwall Block
W-trending basement fabric
Shear zone reflectivity
NE-trending fault (independent of shear zone)

Figure 13

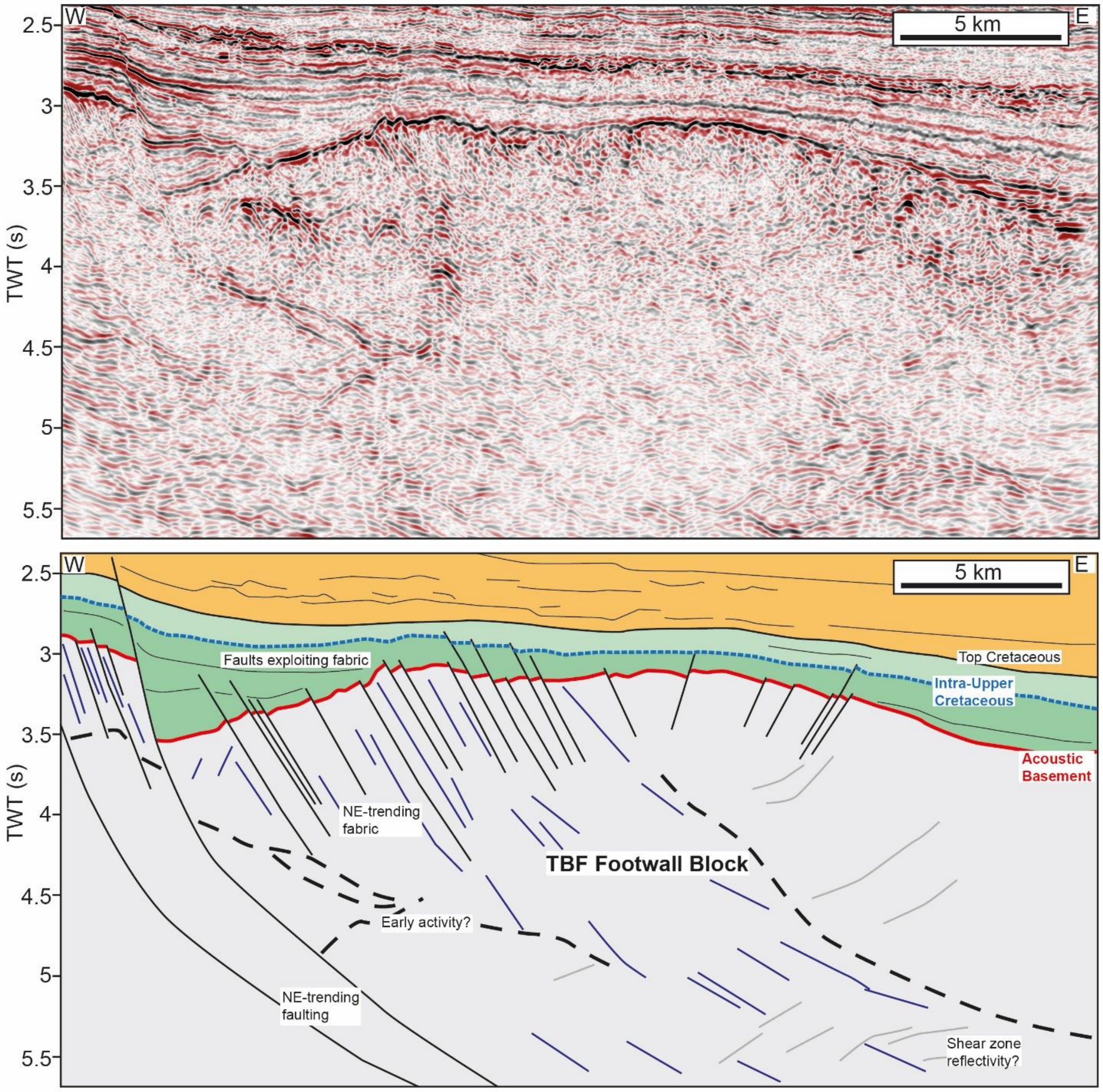
W
E
5 km
TWT (s)
2.5
3
3.5
4
4.5
5
5.5
Faults exploiting fabric
Top Cretaceous
Intra-Upper Cretaceous
Acoustic Basement
NE-trending fabric
TBF Footwall Block
Early activity?
NE-trending faulting
Shear zone reflectivity?

Figure 14

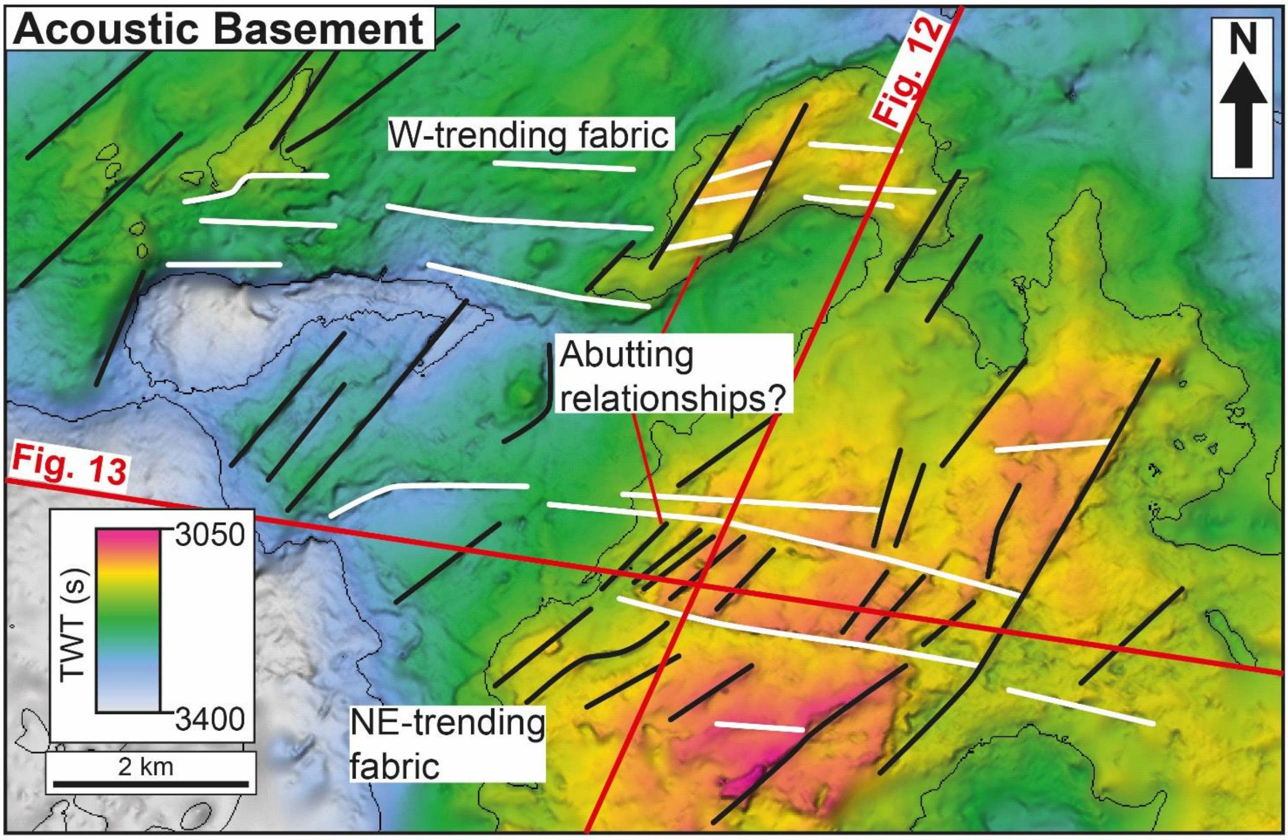
Acoustic Basement
N
Fig. 12
W-trending fabric
Abutting relationships?
Fig. 13
3050
TWT (s)
3400
2 km
NE-trending fabric

Figure 15

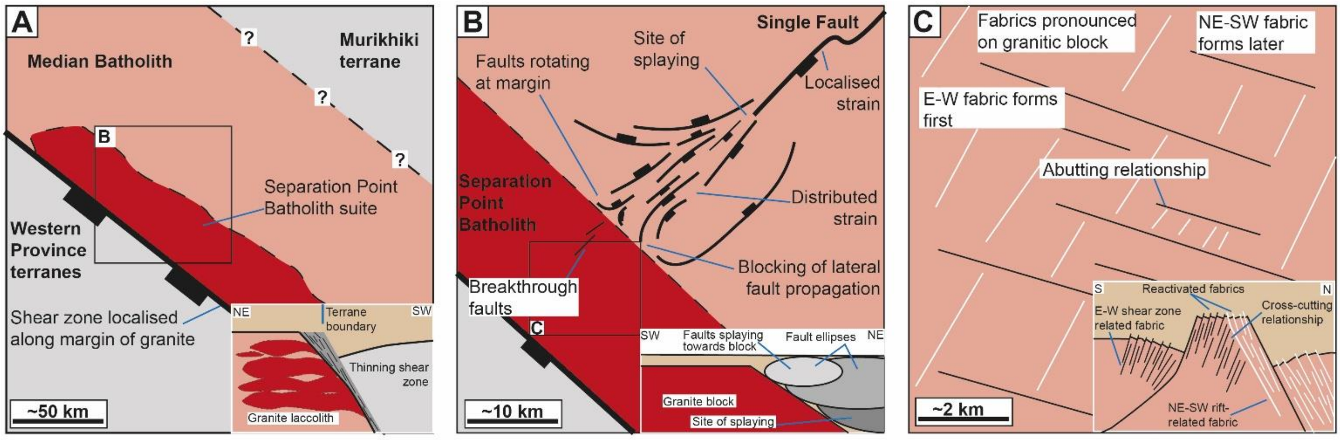
A
Median Batholith
Murikhiki terrane
?
?
?
B
Separation Point Batholith suite
Western Province terranes
Shear zone localised along margin of granite
NE
Terrane boundary
SW
Thinning shear zone
Granite laccolith
~50 km
B
Single Fault
Site of splaying
Faults rotating at margin
Localised strain
Separation Point Batholith
Distributed strain
Blocking of lateral fault propagation
Breakthrough faults
C
SW
Faults splaying towards block
Fault ellipses
NE
Granite block
Site of splaying
~10 km
C
Fabrics pronounced on granitic block
NE-SW fabric forms later
E-W fabric forms first
Abutting relationship
S
Reactivated fabrics
N
E-W shear zone related fabric
Cross-cutting relationship
NE-SW rift-related fabric
~2 km

1349 Figure 16

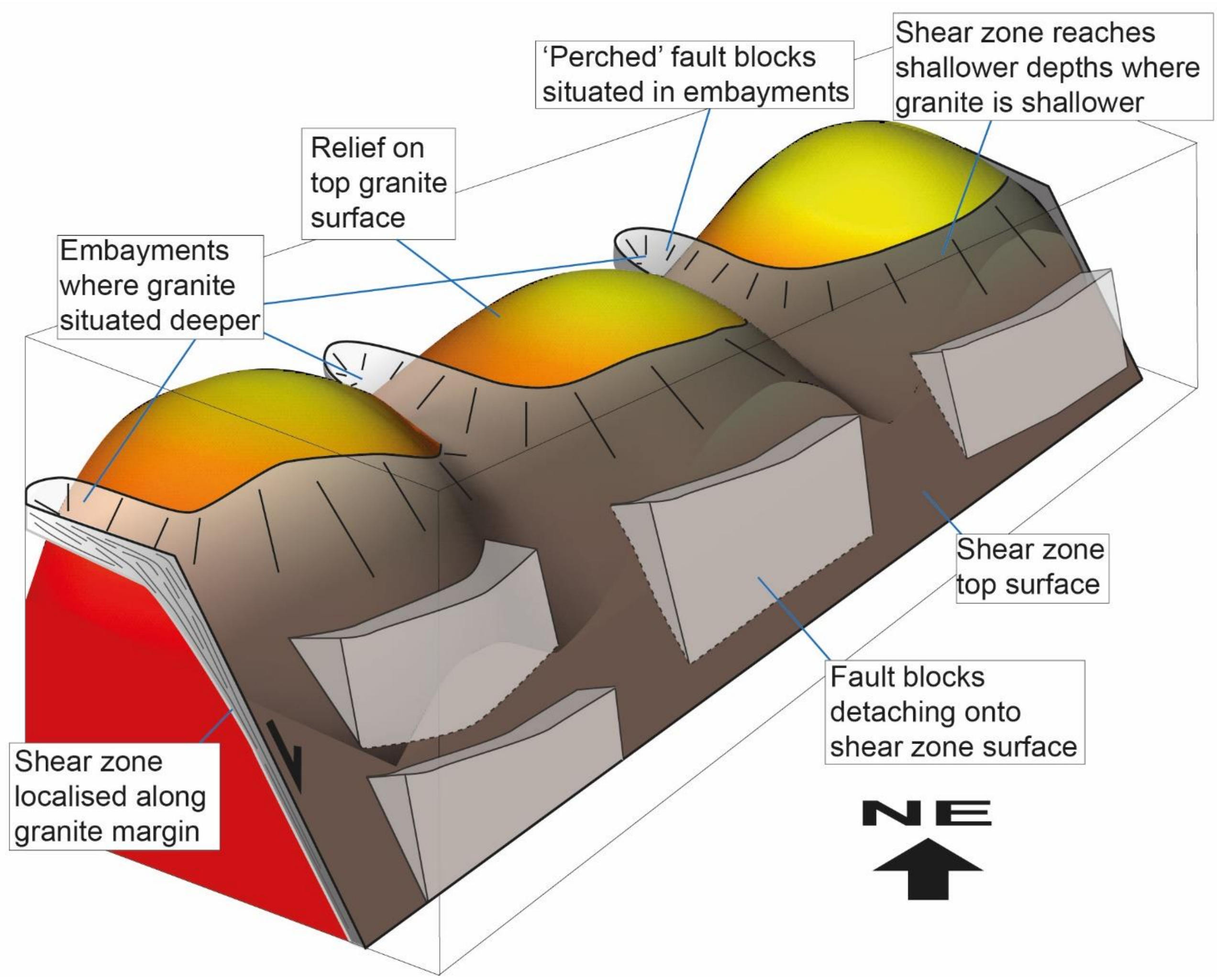

1350